

**Best Available
Copy
for all Pictures**

AD-787 143

**EXPERIMENTAL CHEMICAL LASER MODE
CONTROL**

D. B. Rensch

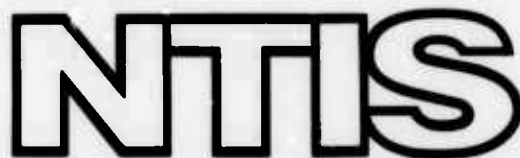
Hughes Research Laboratories

Prepared for:

**Army Missile Command
Defense Advanced Research Projects Agency**

October 1974

DISTRIBUTED BY:



**National Technical Information Service
U. S. DEPARTMENT OF COMMERCE
5285 Port Royal Road, Springfield Va. 22151**

Effective: 16 March 1974
Expiration: 15 August 1974
Amount: \$98,471.00
Program Code Number: 4E20

This research was supported by the Advanced Research Projects Agency of the Department of Defense and was monitored by the U.S. Army Missile Command under Contract Number DAAH01-74-C-0596.

The views and conclusions contained in this document are those of the authors and should not be interpreted as necessarily representing the official policies, either expressed or implied, of the Advanced Research Projects Agency or the U.S. Government.



ii

UNCLASSIFIED

SECURITY CLASSIFICATION OF THIS PAGE (When Data Entered)

DD FORM 1 JAN 73 1473 EDITION OF 1 NOV 65 IS OBSOLETE

UNCLASSIFIED

SECURITY CLASSIFICATION OF THIS PAGE (When Data Enclosed)

UNCLASSIFIED

SECURITY CLASSIFICATION OF THIS PAGE(When Data Entered)

for uniform medium conditions as well as perturbed conditions where significant phase perturbation were introduced into the optical resonator. Extensive medium diagnostics were performed on the DF-CO₂ laser and the results presented.

ia

UNCLASSIFIED

SECURITY CLASSIFICATION OF THIS PAGE(When Data Entered)

TABLE OF CONTENTS

LIST OF ILLUSTRATIONS	3
I INTRODUCTION AND SUMMARY	7
II EXPERIMENTAL APPROACH	11
III EXPERIMENTAL SYSTEM	19
A. Laser	19
B. Resonator Alignment Optics	25
IV LASER MEDIUM PROPERTIES	29
A. Small-Signal Gain	29
B. Medium Homogeneity	40
V EXPERIMENTAL AND THEORETICAL RESULTS	53
A. Beam Quality Measurements	53
B. Resonator Calculations Using the Step-By-Step Propagation Algorithm	60
C. Experimental Results for Perturbed Unstable Resonators	70
D. Discussion of Experimental and Theoretical Results	74
REFERENCES	77

LIST OF ILLUSTRATIONS

Fig. II-1. Schematic showing optical train used to measure beam quality of unstable resonators	14
Fig. II-2. Diagram showing physical dimensions of grooves used to introduce phase perturbations into unstable resonators	16
Fig. III-1. Ten liter pulsed chemical laser	20
Fig. III-2. Ten liter pulsed chemical laser	21
Fig. III-3. Gas control system for 10 liter pulsed laser	24
Fig. III-4. Alignment system for unstable resonators	26
Fig. IV-1. Schematic of small-signal gain measurements for flash photolysis $DF-CO_2$	30
Fig. IV-2. Diagram showing window locations used to measure small-signal beam in $DF-CO_2$ laser	32
Fig. IV-3. Oscilloscope traces of gain and flashlamp profiles	35
Fig. IV-4. Axial small-signal gain for four transverse locations in a flash photolysis $DF-CO_2$ laser	36
Fig. IV-5. Axial small-signal gain for four transverse locations in a flash photolysis $DF-CO_2$ laser	38
Fig. IV-6. Holographic experimental set-up	42
Fig. IV-7. Diagram showing window location used to measure medium homogeneity in $DF-CO_2$ laser	45

Preceding page blank

Fig. IV-8.	Hologram for $F_2:D_2:CO_2:He = 1.5:1:5:10$ mixture at 200 Torr	46
Fig. IV-9.	Hologram for $F_2:D_2:CO_2:He = 1.5:1:5:10$ mixture at 200 Torr	46
Fig. IV-10.	Holograms for $F_2:D_2:CO_2:He = 1.5:1:5:10$ mixture at 200 Torr	47
Fig. IV-11.	Holograms for $F_2:D_2:CO_2:He = 1.5:1:5:10$ mixture at 200 Torr	48
Fig. IV-12.	Holograms for $F_2:D_2:CO_2:He = 1.5:1:5:10$ mixture at 200 Torr	48
Fig. IV-13.	Interferometric holograms for $F_2:D_2:CO_2:He = 1.5:1:5:10$ mixture at 200 Torr	50
Fig. IV-14.	Interferometric holograms for $F_2:D_2:CO_2:He = 1.5:1:5:10$ mixture at 200 Torr	50
Fig. IV-15.	Interferometric holograms for $F_2:D_2:CO_2:He = 1.5:1:5:10$ mixture at 300 Torr	51
Fig. IV-16.	Interferometric holograms for $F_2:D_2:CO_2:He = 1.5:1:5:10$ mixture at 300 Torr	51
Fig. V-1.	Far-field mode patterns for unstable resonator with geometric magnification $m = 2.1$	54
Fig. V-2.	Comparison of measured and ideal integrated far-field power for confocal unstable resonator	55
Fig. V-3.	Comparison of measured and ideal integrated far-field power for confocal unstable resonator	57
Fig. V-4.	Comparison of measured and ideal integrated far-field power for confocal unstable resonator	58

Fig. V-5.	Far-field mode patterns for $N_{eq} = 1.5, M = 1.2 \dots \dots \dots \dots$	59
Fig. V-6.	Calculated mode distribution for confocal unstable resonator	61
Fig. V-7.	Calculated mode distribution for confocal unstable resonator	62
Fig. V-8.	Diagram showing profile used in computer program to simulate mirror groove for phase pertur- bation study	66
Fig. V-9.	Calculated mode distribution for confocal unstable resonator	67
Fig. V-10.	Calculated mode distributions for confocal unstable resonator	69
Fig. V-11.	Near-field mode pattern for unstable resonator mirrors	71
Fig. V-12.	Far-field mode pattern for unstable resonator with grooved mirrors	71
Fig. V-13.	Comparison of calculated and measured far-field power for perturbed unstable resonator	72
Fig. V-14.	Comparison of calculated and measured far-field power for perturbed unstable resonator	73

I. INTRODUCTION AND SUMMARY

Since June 1970, Hughes Research Laboratories has carried out mode control studies for high power lasers under the Chemical Laser Mode Control program, funded by ARPA through the Army Missile Command (Contract Nos. DAAH01-70-C-1086, DAAH01-72-C-0067 and DAAH01-73-C-0290). At the present time, mode control is recognized as a difficult but essential part of all high power laser design. Many valuable modeling techniques which are presently used in designing mode-controlled oscillators for high power lasers were developed under the Chemical Laser Mode Control program.

Up to this time, the work carried out on this program has been theoretical rather than experimental. Now that the necessary analytical techniques and approximations have been developed and verified by comparison with the few experiments that are available, it is desirable to apply this knowledge in the most efficient way to the problems of practical laser devices.

The experimental effort described in this report has been directed mainly at determining the operating behavior of unstable resonators at different Fresnel numbers. Interest in the operational behavior of unstable resonators at various Fresnel numbers was first generated by Siegman and Arrathoon¹ when they verified that the periodic variation of the lowest-loss mode actually represented a periodic crossing over of mode losses. At each mode loss crossing, a different and distinct eigenmode becomes the lowest-order or lowest-loss mode of the resonator. The modes are degenerate in loss at the crossing, but are still distinct. Siegman² demonstrated that the crossing points for the lowest loss axially symmetrical ($l = 0$) modes in circular resonators occur very nearly at integer values of equivalent Fresnel number N_{eq} (for a positive branch confocal unstable resonator with a large mirror diameter $2a_2$ the equivalent Fresnel number is given by $N_{eq} = \left\lceil (M-1)/2M^2 \right\rceil N_0$, where M is the geometric magnification, $N_0 = a_2^2/L\lambda$ is the conventional resonator Fresnel number, and L is the mirror separation), while maximum separation occurs

Preceding page blank

at integer plus one-half values. The eigenvalues for higher-order modes having azimuthal as well as radial variations also interleave with each other and show no termination of this crossing behavior as the resonator Fresnel number increases.

Because of this periodic behavior of the eigenmodes versus Fresnel number, speculation arises as to the important of designing the laser resonator system to have an N_{eq} equal to an integer plus one-half in order to achieve maximum mode discrimination. Both geometric³ and diffraction analysis^{4,5} have shown that the fundamental mode of an unstable resonator can provide fundamental modes with large volume, nearly uniform intensity and phase distributions. Those ideal characteristics result in maximum laser far-field brightness. This same analysis has also shown that the higher order symmetric modes do not have the same ideal characteristics. The intensity and phase distributions are not uniform for these modes. For this reason, the designer of a resonator system often chooses integer plus one-half values for N_{eq} in order to avoid the higher order modes.

The type of analysis referred to above for finding the eigenmodes and eigenvalues of unstable resonators is not directly applicable to finding the mode or modes of a laser that will reach oscillating threshold in the presence of a laser medium. Therefore, while these techniques have been able to determine the individual characteristics of the fundamental and higher-order modes, they have not answered the question as to what modes will actually reach oscillating threshold in the presence of a laser medium. The type of analysis which can answer this question is a Fox and Li type iteration which we have used throughout the Chemical Laser Mode Control program.⁶⁻⁹ It has been our belief after making numerous unstable resonator calculations which included uniform and nonuniform gain, medium density perturbations, and mirror misalignment that single mode operation is independent of resonator Fresnel number. In other words, the beam characteristics of the resonator will not significantly change if the equivalent Fresnel number is changed by a half-integer.

It is the purpose of this experimental study to verify that our analytical computer techniques are accurate in predicting a non-dependence of beam quality on half-integer steps in Fresnel number. To date, there is only one known report of experimental measurements where a dependence was found.¹⁰ Here, the authors report near-diffraction limited operation for output couplings from 34% to 85%, with a sensitivity to the value of equivalent Fresnel number being found only for the lowest output coupling. In our study, the beam quality for three output couplings 77%, 50%, and 30% are measured versus integer and half-integer values of equivalent Fresnel number. Small signal gains as high as 22 dB/roundtrip, intentional phase perturbations with a maximum optical phase shift of 1.4 rad, were used in the study to determine if the output beam characteristics of unstable resonators are sensitive to the value of equivalent Fresnel number.

The active medium used in the study was a flash-photolysis D₂-F₂-CO₂ chemical laser. The laser system provided measured peak gains of approximately 2.5%/cm near the center of the cavity with pulse lengths to 70 to 80 μ s. The medium density uniformity was measured to be greater than $\lambda/9$ for essentially the entire laser pulse (we found that detonation waves emanating from the flashlamp eventually propagated into the laser medium and destroyed medium uniformity).

During our study we did not find any dependence of Fresnel number on the beam quality of unstable resonators. These results also include the 30% output coupling configuration. Measured far-field power in the central and side lobes were found to be in good agreement with diffraction limited results for nonperturbed resonators, and in good agreement with calculated results for resonator configurations where phase perturbations were intentionally introduced.

The following sections give the details of the experimental study. Section II describes the experimental approach. Section III describes the laser system and resonator alignment technique. Section IV describes the experimental procedure used to measure small-signal gain and medium density uniformity, and discusses the results of these measurements. Section V discusses the results of the beam quality measurements versus resonator equivalent Fresnel number.

II. EXPERIMENTAL APPROACH

To determine if the output beam quality of an unstable resonator depends on output coupling as well as Fresnel number, we chose three different output couplings and various resonator equivalent Fresnel numbers for each coupling. All resonator configurations were confocal, and belonged to the positive branch. The lowest coupling loss chosen was 30% ($M = 1.2$). Typically unstable resonators are designed and used at higher couplings because of their inherent sensitivity to mirror misalignment and medium density inhomogeneities at low couplings.⁹ We wanted to choose a coupling similar to the 34% used in Ref. 10, where they found a beam quality dependence on Fresnel number. The other two loss couplings used in the study were 50% ($M=1.41$) and 77% ($M = 2.1$). The highest coupling was set by the maximum gain we expected to obtain in the laser medium.

We chose the resonator equivalent Fresnel numbers to be between 0.8 and 2.5 (the conventional Fresnel number range is 8 to 20). We decided on low resonator Fresnel number values because the small Fresnel number resonators occupy a relatively small volume in the center of the laser cavity where the laser medium is expected to be more nearly uniform in gain and density. Table II-1 lists the equivalent Fresnel numbers and corresponding resonator dimensions used in the experimental study.

The active medium that we used for the unstable resonators was a flash photolysis DF-CO₂ chemical laser (See Section III for a detailed description of the laser device). The laser is a single-shot, static-flow device. The total length of the active region is 100 cm and the available volume is 10 liters. The chemical reaction which provides gain on the CO₂ (001) - CO₂ (100) transition is initiated by two flashlamps located on opposite sides of the cavity. Because of the nonsymmetrical initiation configuration, some spatial gain and medium

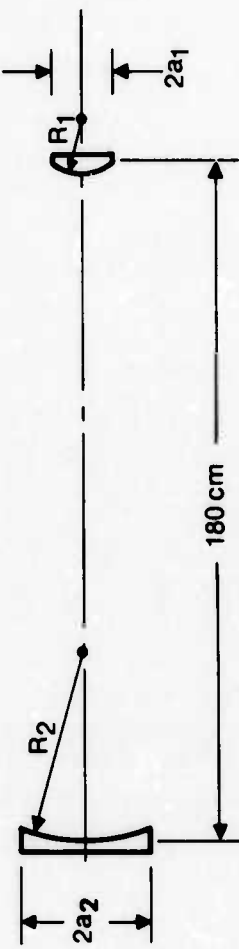
Preceding page blank

TABLE II-1
Resonator Parameter Used in Experimental Study

Coupling Loss	30%			50%			77%			
	N_{eq}	1.2	1.5	0.87	1.02	1.2	1.4	1.6	2.10	2.5
a_1 (cm)	1.50	1.67	0.86	0.97	1.05	1.14	1.22	0.85	0.93	
a_2	1.80	2.00	1.21	1.37	1.49	1.61	1.72	1.79	1.96	
R_1	-1800	-1800	-870	-870	-870	-870	-870	-328	-328	
R_2	2160	2160	1230	1230	1230	1230	1230	690	690	

T1441

3569-1



density nonuniformity were expected. As we have shown in earlier reports^{6, 7} medium density uniformity, and to a lesser degree, gain uniformity are important in obtaining good beam quality. Therefore, in order to accurately interpret beam quality results obtained later in the experimental study, gain and medium density measurements were made.

Gain measurements at various locations across the laser cavity were made using a small diameter probe beam from a CO₂ laser. The gain at a particular location was recorded starting at the discharge of the flashlamp capacitors and continued throughout the positive portion of the gain. For each location the effect of cavity pressure and flashlamp input energy on gain was determined. Details of the experimental setup and results are given in Section IV-A.

Medium density homogeneity measurements were made using double-exposure pulsed holographic interferograms. Because of cavity symmetry, the holograms covered only one-quarter of the 10 cm x 10 cm cavity cross section. Holograms were made using the same gas mixtures, cavity pressures, and flashlamp input energies used for the gain measurements. They were recorded at approximately 10 μ s intervals beginning at the start of the flashlamp. Details of the experimental setup and results are given in Section IV-B.

Next, we measured the beam quality of the 77%, 50%, 30% loss coupled unstable resonators listed in Table II-1. The procedure we used to measure beam quality for a particular resonator N_{eq} and output coupling was to accurately align the resonator using a He-Ne laser and optical train described in Section III-B. The laser was fired and the beam from the resonator was coupled out of the cavity through a KCl window and reflected off a flat mirror containing a linear reflection grating on the front surface. The grating groove period was designed to give only one diffraction order at 18 degrees from the grating normal, and the groove depth was set to give approximately 6% of the incident energy in this order. The diffracted energy was directed onto two diffuse scatterers and detected by a HgCdTe detector (see Fig. II-1). The signal from the detector was used to monitor total

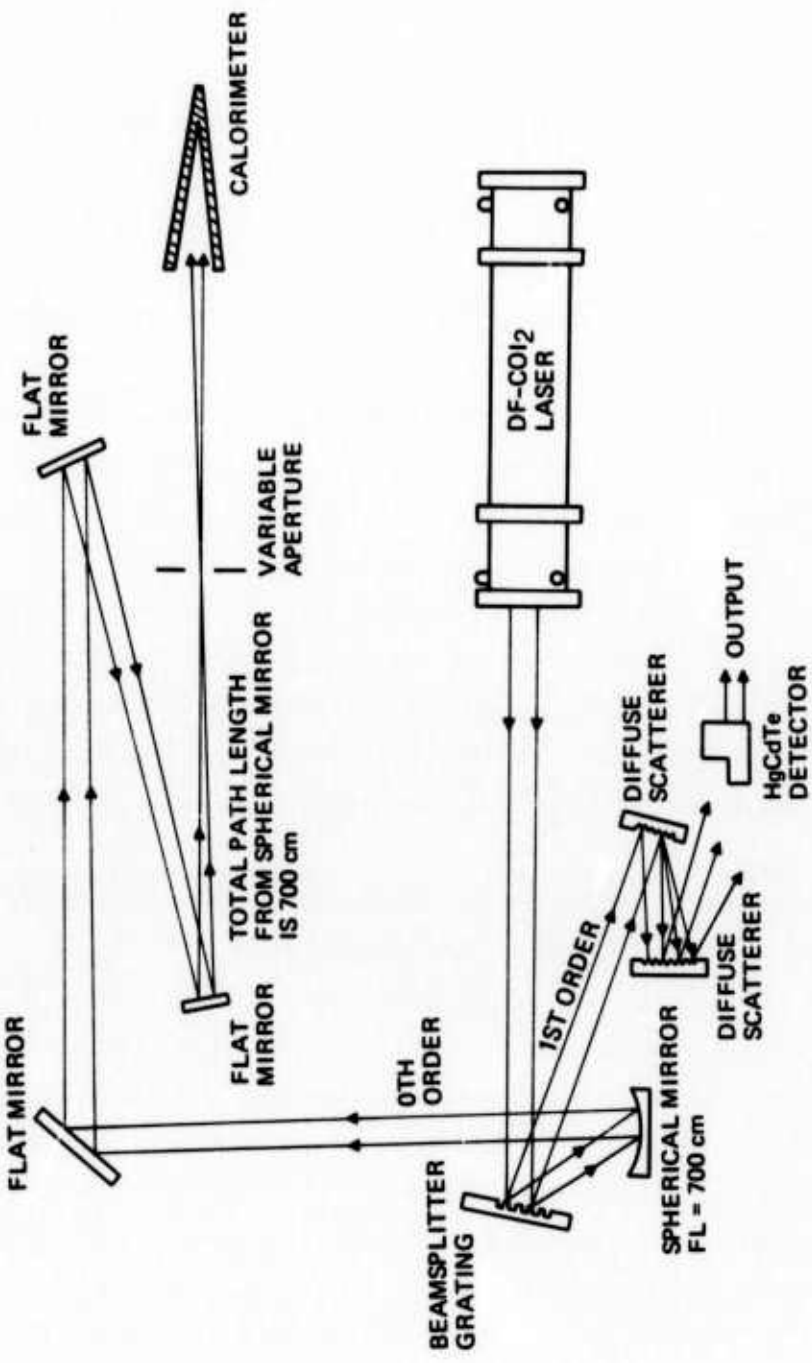
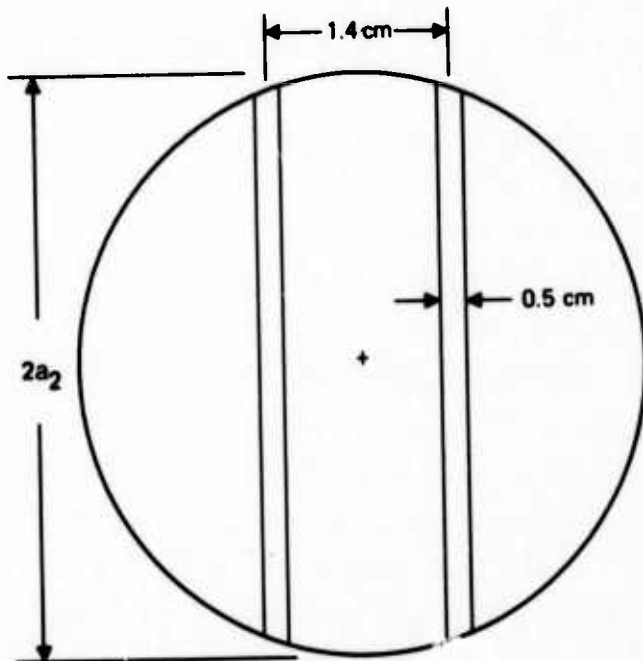


Fig. II-1. Schematic showing optical train used to measure beam quality of unstable resonators.

near-field power. The HgCdTe detector was calibrated for power measurements by placing a calorimeter in the beam reflected from the grating (0th order), and comparing the signal obtained from the calorimeter with the total area under an oscilloscope trace of the detector output.

The reflected beam from the grating was reflected off a spherical mirror with a focal length of 700 cm, folded back and forth via four flat mirrors for a total propagation length of 700 cm, passed through a variable aperture, and finally absorbed by a calorimeter. Total far-field power is measured with the calorimeter by removing the aperture. The output signal from the calorimeter was compared with the signal simultaneously obtained from the near-field detector. Beam quality was obtained by measuring the amount of power transmitted through a given aperture size and comparing it with the amount of power that would have been transmitted had the near-field beam been uniform in intensity and phases (diffraction limited). It should be noted here that because reflection gratings are sensitive to the polarization of the incident beam, we were required to assure that the output of the laser maintained a constant polarization. We did this by ion machining a grating onto the surface of the resonator's large mirror. The groove period and depth was 12.5 μm and 0.35 μm , respectively. The grating at incident angle diffracts 0.25% of the parallel polarized radiation and 1.5% of the perpendicular. This gives a polarization discrimination ratio of 6 to 1. The grating introduces a loss of $2 \times 0.25 = 0.5\%$ in the resonator.

Following the beam quality measurements for the various resonators listed in Table II-1, we intentionally introduced a known phase perturbation into the cavity of the 77% and 30% output coupled resonators and measured the resulting beam quality. The phase perturbations were two parallel grooves, ion-machined into the resonator's large mirror as shown in Fig. II-2. Width of the grooves and distance from the center of the resonator were scaled to be similar to the shock waves that exist in gas dynamic lasers (GDL). Depth of the



GEOMETRIC OUTPUT		
COUPLING:	30%	77%
R _m	0.8 rad	1.2 rad

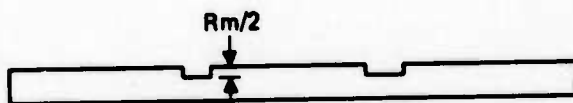


Fig. II-2. Diagram showing physical dimensions of grooves used to introduce phase perturbations into unstable resonators.

grooves were fixed to give a total phase shift R_m of 0.8 rad and 1.2 rad, respectively, for the 30% and 77% output coupled resonators. These depths were chosen after modeling the phase perturbed resonators with our three-dimensional step-by-step resonator computer program. Details and results of the computer modeling and beam quality measurements are given in Section V-B and V-C.

III. EXPERIMENTAL SYSTEM

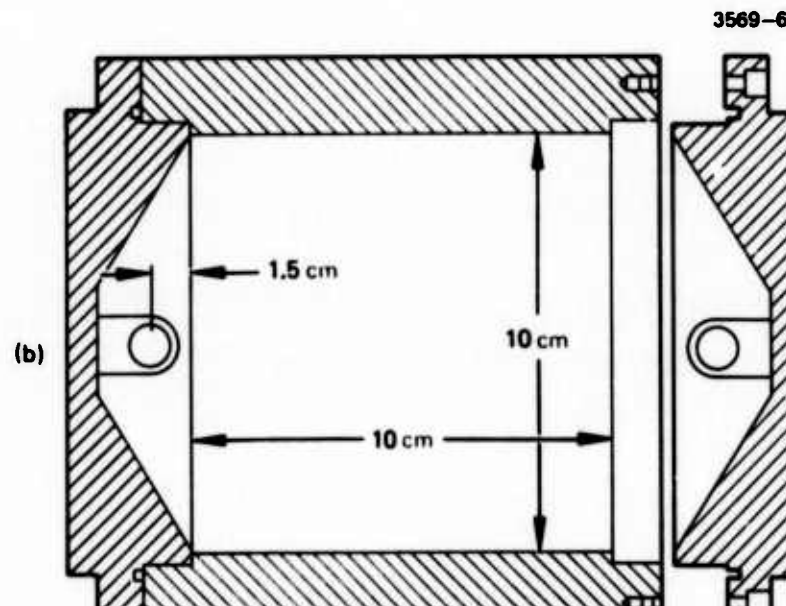
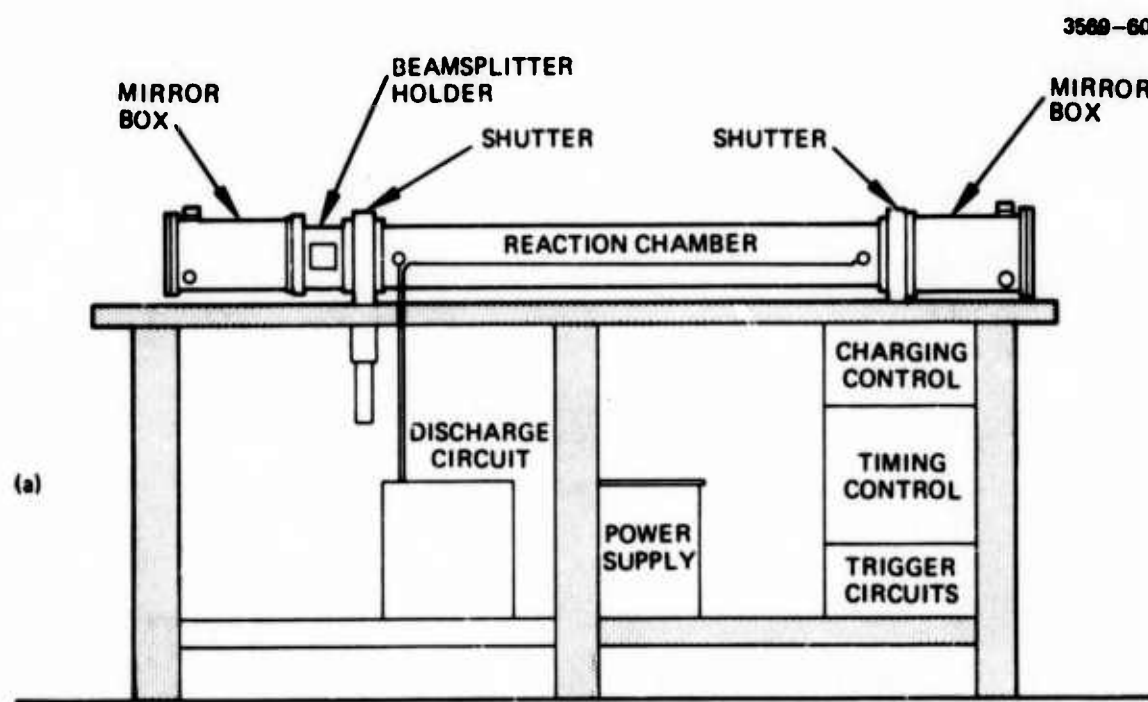
A. Laser

The laser system that we used to perform the experimental mode control studies is comprised of a modular laser head, a gas filling system, energy discharge circuits, and a control and timing circuit. Figure III-1 shows the physical layout of the laser system and a cross-sectional view of the laser cavity.

The modular laser head is made of aluminum and is designed for maximum flexibility. The various components identified in Fig. III-1(a) are bolted together with O-ring seals, and each component can be replaced easily to reconfigure the laser.

For this study, the laser used two xenon flashlamps (100 cm length, 1.25 cm diameter) located on opposite sides of the laser cavity. The flashlamps are located inside the reaction volume, but are outside of the actual laser cavity. The effective laser cavity volume is 10 cm x 10 cm x 100 cm long for a total volume of 10 liters. The small volumes that surround each flashlamp and are located outside the laser cavity are broken up by radiation absorbing partitions to prevent parasitic oscillations in these regions. The walls of the laser cavity and flashlamp holders are coated with aluminum oxide to give low reflectivity at 10.6 μ m, and high reflectivity at ultraviolet wavelengths. Two 1-in. diameter vacuum pumping lines are connected to the reaction column to provide rapid evacuation of the reacted gas mixtures following a laser pulse.

Because fluorine is detrimental to mirror coatings, provision is made to isolate the reaction chamber from the mirrors until immediately before the chemical reaction is initiated by the flashlamps. Isolation is achieved by a sliding stainless steel shutter blade at each end of the reaction chamber. The shutter blades are driven by pneumatic cylinders. In the closed position the shutters are seated against teflon sealing rings. These shutters are not intended to be vacuum tight, but merely to reduce the flow conductance between the reaction chamber and the mirror boxes to a small value. The reaction chamber and shutter assemblies are shown in Fig. III-2.



TEN LITER PULSED CHEMICAL LASER
 (a) PHYSICAL LAYOUT
 (b) CAVITY CROSS SECTION

Fig. III-1. Ten liter pulsed chemical laser. (a) Physical layout. (b) Cavity cross section.

M9560

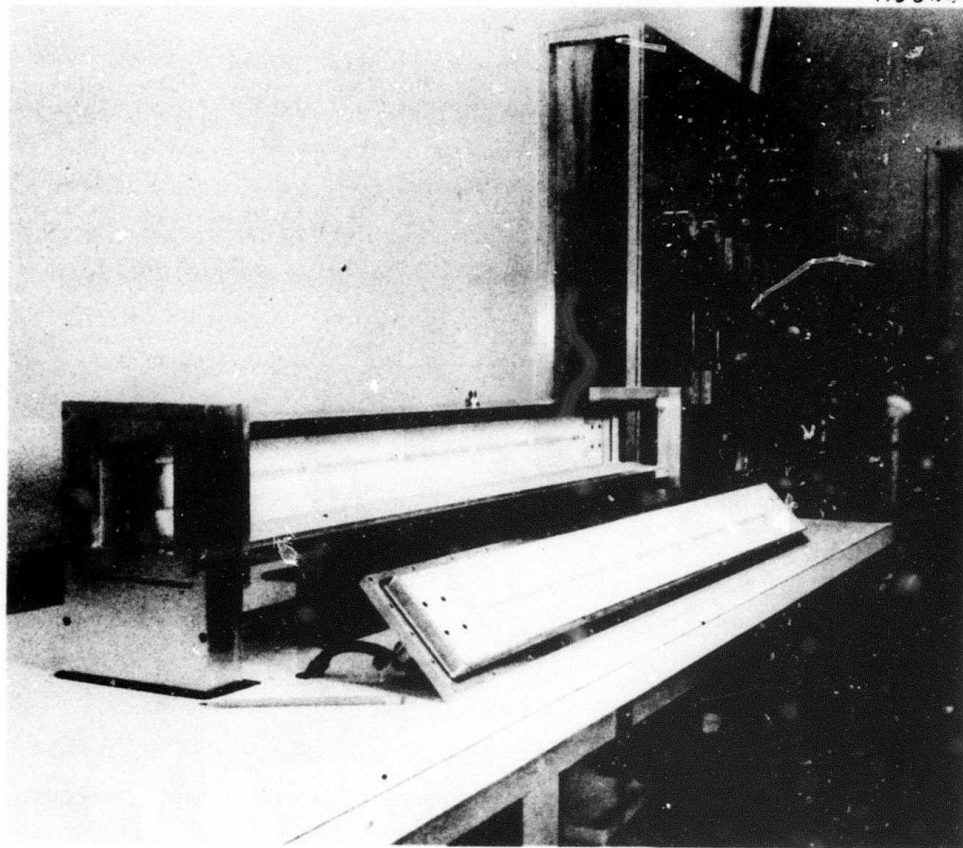


Fig. III-2. Ten liter pulsed chemical laser.

The vacuum integrity of the laser head is provided by the mirror and beam splitter boxes. The resonator mirrors are located within the laser head to minimize the need for large high quality windows. Each mirror box is provided with its own gas supply and vacuum pump system. During the filling of the reaction chamber the mirror and beam splitter boxes are simultaneously filled with an inert mixture of gases (e.g., argon and helium) at a rate that maintains a minimum pressure difference across the shutters. The beam splitter box provides a convenient location to insert a beam splitter into the optical cavity in order to sample the right and left traveling cavity fields. Two windows located opposite each other allow the two sampled beams to be removed.

The laser resonator mirrors are held by a three-point kinematic suspension that is anchored to the mirror box wall. The mirror box and laser head are sufficiently rigid so that once the cavity and mirror regions have reached their final operating pressure, adequate resonator structural support is provided. Adjustment of the resonator mirrors is provided by screws which set on two of the suspension points. These screws can provide an alignment tolerance of better than $\pm 10 \mu\text{rad}$. The screws are driven from outside the box through a rotary vacuum feedthrough.

The gas handling system performs the following functions:

1. Provides accurate known proportions of each gas
2. Ensures complete mixing of the gases
3. Permits accurate filling of the device to any pressure
4. Provides inert gas filling of the mirror boxes simultaneous with filling of the reaction chamber.

Because of the large volume it is not feasible to make up mixtures external to the laser volume, nor is it feasible to provide stirring in the reaction chamber to ensure complete mixing. For this reason a dynamic filling system is used. The flow rate of each gas component is controlled by brass valves and monitored by Brook's flowmeters.

Prior to filling the laser cavity, each valve is pre-set to give the desired flow rate. The individual flow rates are set according to the desired mixture ratio. To fill the reaction chamber, all the flows are turned on simultaneously. The gas flows through a sufficient length of feed line so that turbulent mixing is complete before the gas mixture enters the reaction chamber. Filling is stopped by the experimenter when the pressure has reached its desired value. The total flow rate is chosen so the filling time is approximately 30 s. The gas control system can be seen in the background of Fig. III-2 and is shown schematically in Fig. III-3.

The flashlamp discharge circuits use conventional ignitron switches to discharge a $7.5 \mu\text{F}$ capacitor through each flashlamp. At full rated voltage (15 kV) the total input energy is 1.7 kJ. Experimental results show that the lamps will work reliably at voltages of 9 kV and above; therefore, for parametric investigations we can operate with input energies as low as 0.6 kJ using one flashlamp. The present flashlamp circuitry produces flashlamp pulses with half-widths of about 20 μs .

The control and timing circuits operate the various pneumatic mechanisms and the flashlamp discharge is a rapid, fixed sequence to ensure minimum damage to the internal optical components from attack by F_2 or DF. The operating sequence for the laser is as follows:

	<u>Reaction Volume and Mirror Boxes</u>	<u>Vacuum Pumpout Valve</u>	<u>Shutters</u>
1. Start fill	Evacuated	Closed	Closed
2. Stop fill	At final pressure	Closed	Closed
3. Charge	At final pressure	Closed	Closed
4. Depress "fire" capacitors	At final pressure	Closed	Opening
5. Shutters open	Lasing	Opening	Open

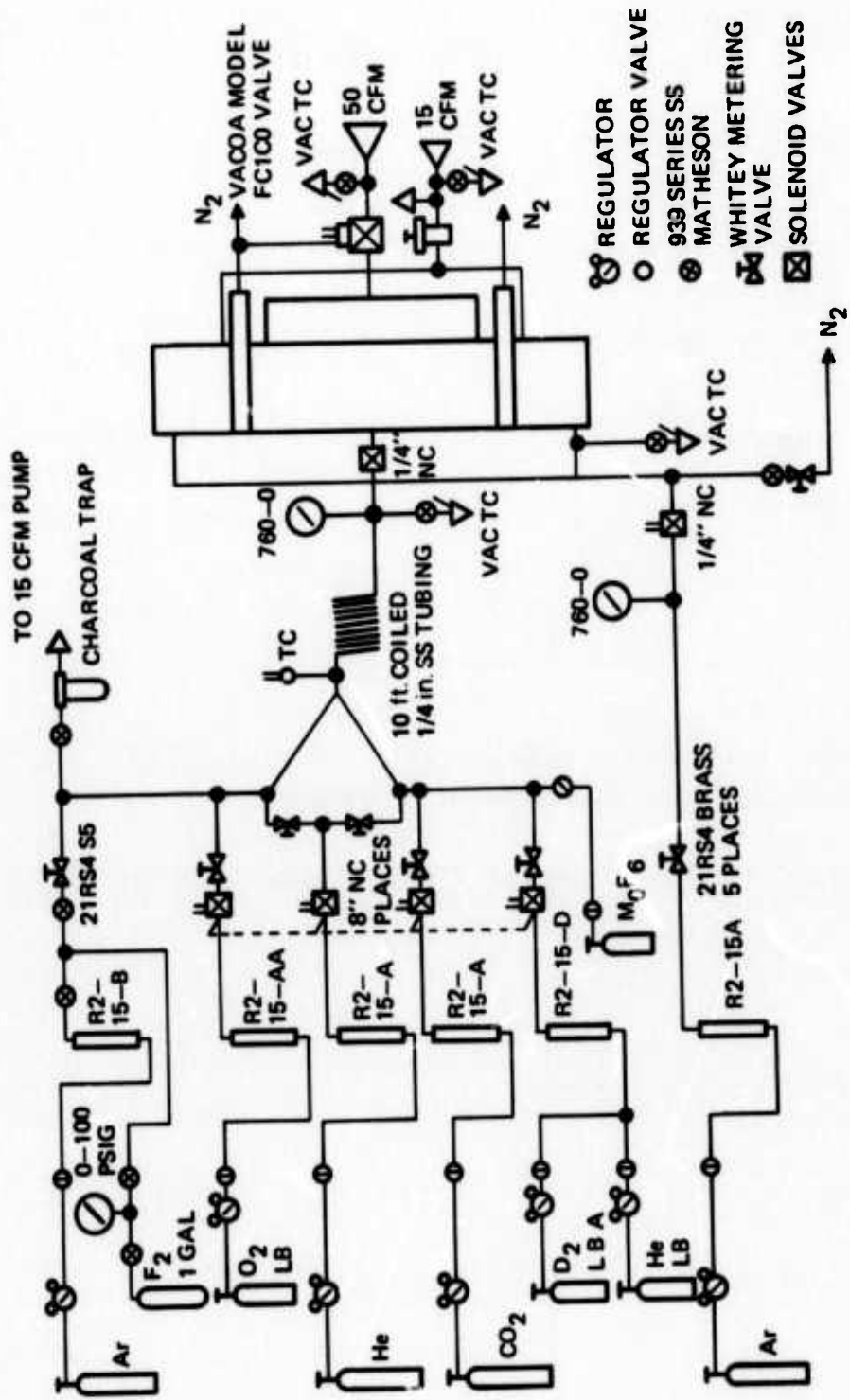


Fig. III-3. Gas control system for unstable resonators.

	<u>Reaction Volume and Mirror Boxes</u>	<u>Vacuum Pumpout Valve</u>	<u>Shutters</u>
6. Pumpout	Common evacuation	Open	Open
7. Purge phase	Purge on separate evacuation	Open	Closed

Steps 4 through 6 of this sequence are performed automatically when the "FIRE" button is depressed. The remaining operations are performed manually by the experimenter. Triggering of the flashlamp is controlled by microswitches at the end of the shutter travel. This prevents reaction initiation until both shutters are completely retracted out of the cavity.

B. Resonator Alignment Optics

Alignment systems for resonator optics on cw or repetitively pulsed lasers do not have to be complex for these lasers. Once the resonator optics are sufficiently aligned to permit lasing, the operator can fine tune the mirror to optimize the near and far field of the laser beam. For single-shot pulsed laser systems, however, the operator must be able to accurately align the laser before each shot. The alignment system we used is schematically shown in Fig. III-4. The output from a He-Ne laser is focused through a pinhole aperture and allowed to expand to a diameter of 12 cm before being recollimated by a 700 cm focal length mirror. The collimated beam enters the output aperture of the confocal unstable resonator and is focused to a diffraction limited spot in the center of the resonator. Spreading of the beam due to diffraction near the center of the resonator, causes the beam to propagate outward and refill the resonator. The portion of the beam coupled out of the resonator is brought to a focus at the pinhole by mirror M_2 .

The sensitivity of the visible focused spot on the aperture to resonator mirror alignment is nearly identical to that of the actual laser output. In both cases, the center of the resonator is filled by a

3569-4

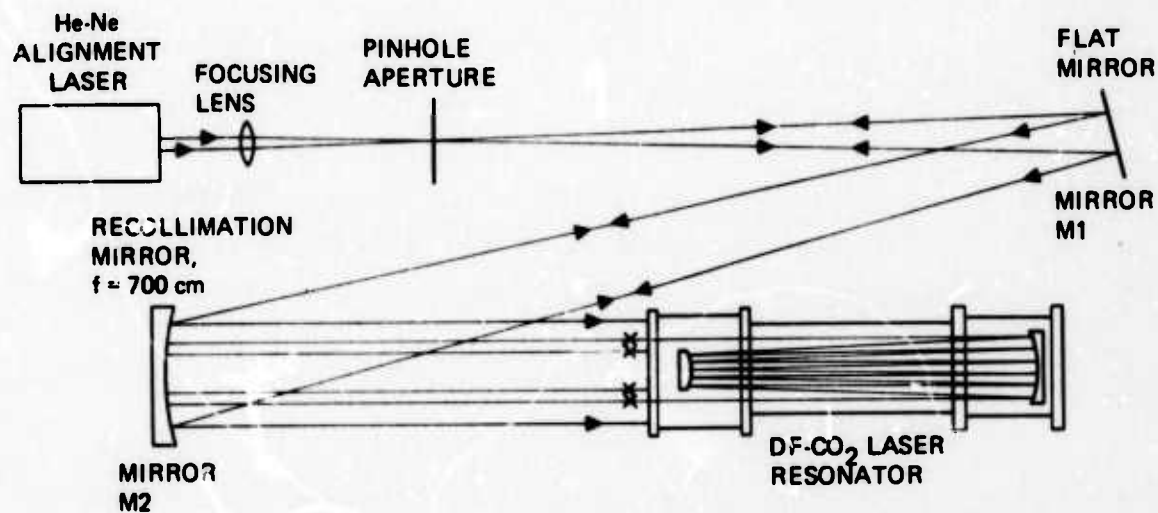


Fig. III-4. Alignment system for unstable resonators.

beam whose diameter is controlled by diffraction, and the number of passes the beam must make before it exits the resonator is determined by the resonator magnification. Therefore, for resonators that are very sensitive to mirror misalignment, such as confocal unstable resonators with low output couplings (e.g., magnifications $M \rightarrow 1$), this alignment procedure automatically increases its sensitivity and permits accurate alignment of the resonator mirrors.

IV. LASER MEDIUM PROPERTIES

A. Small-Signal Gain

1. Experimental Technique

Gain measurements were made by passing the beam from a single transverse mode, single transition, 1/2-W cw CO₂ laser through the DF-CO₂ laser medium and detecting the change in its intensity during the F₂-D₂ chemical reaction pulse. The experimental technique showing the optical path of the CO₂ probe beam and the associated triggering circuit which controls the firing of the flashlamps is shown schematically in Fig. IV-1.

To aid in alignment of the optical components the beam from a He-Ne laser is combined collinearly with the output beam from a small sealed-off CO₂ laser. Both beams are passed through a low-frequency, mechanical chopper, reflected from mirrors M₁ and M₂ which are used to position the beam, and passed through the 100-cm long DF-CO₂ laser medium. When the beams emerge from the cavity, a small 0.6-cm diameter flat mirror M₃ is used to direct the beams onto a Santa Barbara 1 mm x 1 mm HgCdTe detector. The output beam from a second He-Ne laser is used to provide a trigger source to fire the flashlamps. The beam from this laser intersects the CO₂ probe beam at the surface of the mechanical chopper, passes through the chopper, and is detected by an EGG photodiode. The output pulse from the photodiode is differentiated to give a pulse width of 5 μ s and is then amplified to produce a peak voltage of 25 V. The amplified pulse is sent to the laser trigger control system which fires the flashlamps on the 1st pulse received after both shutters in the laser cavity are opened.

In preparation for measuring small-signal gain, the CO₂ probe laser was turned on, tuned to either the P(18) or P(20) transition, and allowed to stabilize. The He-Ne alignment laser was checked for collinearity with the probe beam, M₁ and M₂ were adjusted to permit the probe beam to pass through one of the nine window positions located

Preceding page blank

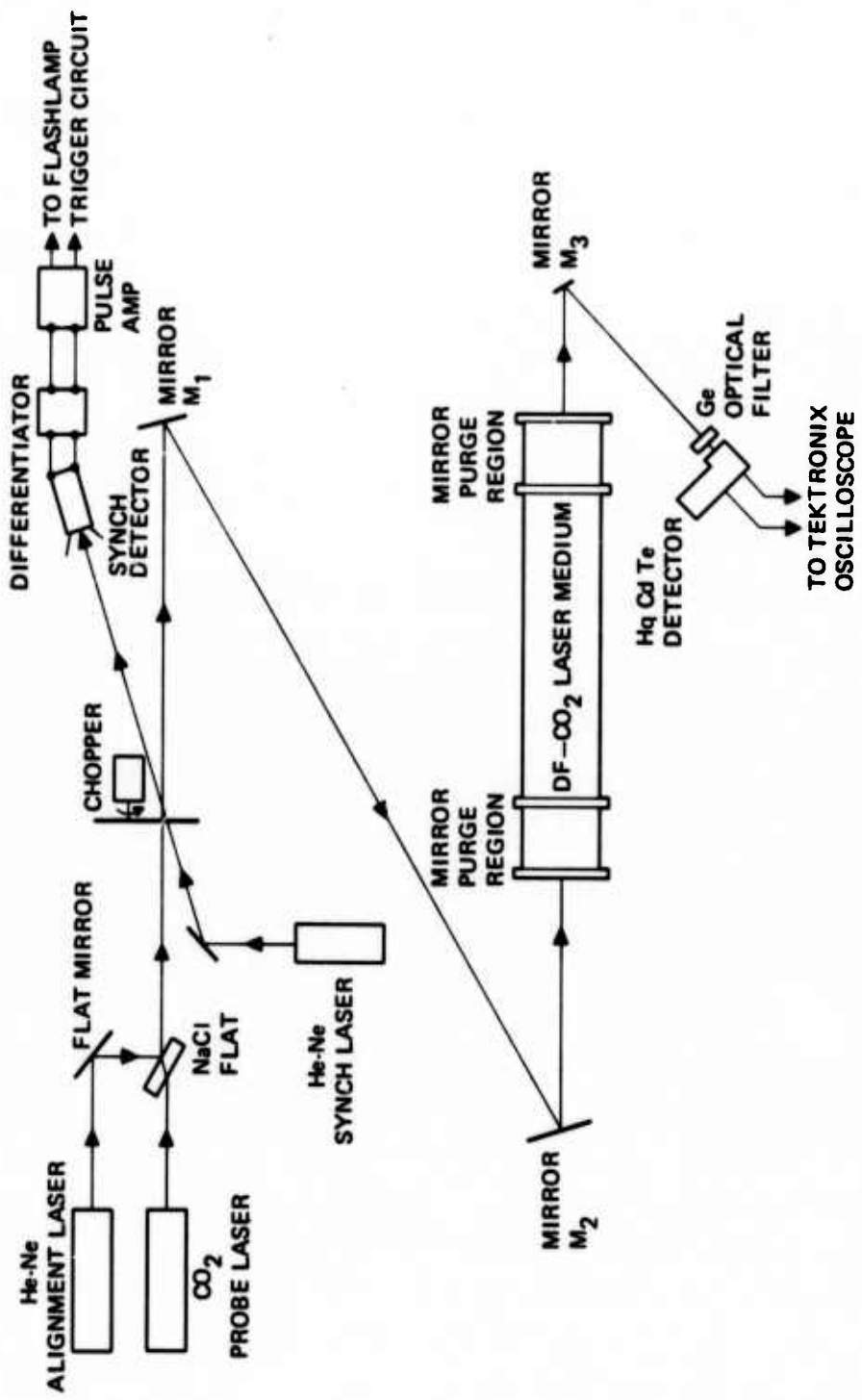


Fig. IV-1. Schematic of small-signal gain measurements for flash photolysis DF-CO_2 .

at the end of the DF-CO₂ cavity (see Fig. IV-2 for window locations), and mirror M₃ was adjusted so that the probe beam illuminated the HgCdTe detector. Following the alignment procedure, the DF-CO₂ laser cavity shutters and vacuum valves were closed, and the flashlamp capacitors charged to the desired voltage (10 kV to 15 kV). Next, the laser cavity and the mirror buffer region were filled to the desired total pressure using pre-set flow meter settings to give the proper mixture ratio. Finally, the fire button was depressed starting the flashlamp firing sequence.

Gain was determined from the ratio of the detector voltage V_e during the chemical reaction and the detector voltage V_o just prior to initiation of the reaction by the flashlamps. All measurements were made with an antireflection coated Ge flat in front of the detector to block radiation from the flashlamps, and anywhere from 1 to 2 fine-meshed stainless steel screens were used as 10.6 μ m attenuators.

This measurement technique was found to be quite reliable for the wide range of medium conditions studied. In the following section, these conditions are given along with the gain results.

2. Experimental Results

In this section the spatial and temporal gain properties of the flash photolysis DF-CO₂ laser are presented. Because of the cavity symmetry when both flashlamps are used to initiate the chemical reaction, gain measurements were made at four locations covering one-quadrant of the cavity (e.g., at locations 5, 6, 8, and 9 in Fig. IV-2). When only one flashlamp is used, six locations are used covering one-half of the cavity.

Table IV-1 lists the F₂:D₂:O₂:CO₂:He mixture ratio, total pressure, number of flashlamps, and flashlamp input energy values used in the gain measurements, and the combination of parameters used for each experimental case studied. A larger percentage of our data was taken at a total pressure of 200 Torr and a F₂:D₂:O₂:CO₂:He = 1.5:1:1:5:10 mixture ratio. We found that a cavity pressure of 200 Torr provided large small-signal gains which are desirable for the

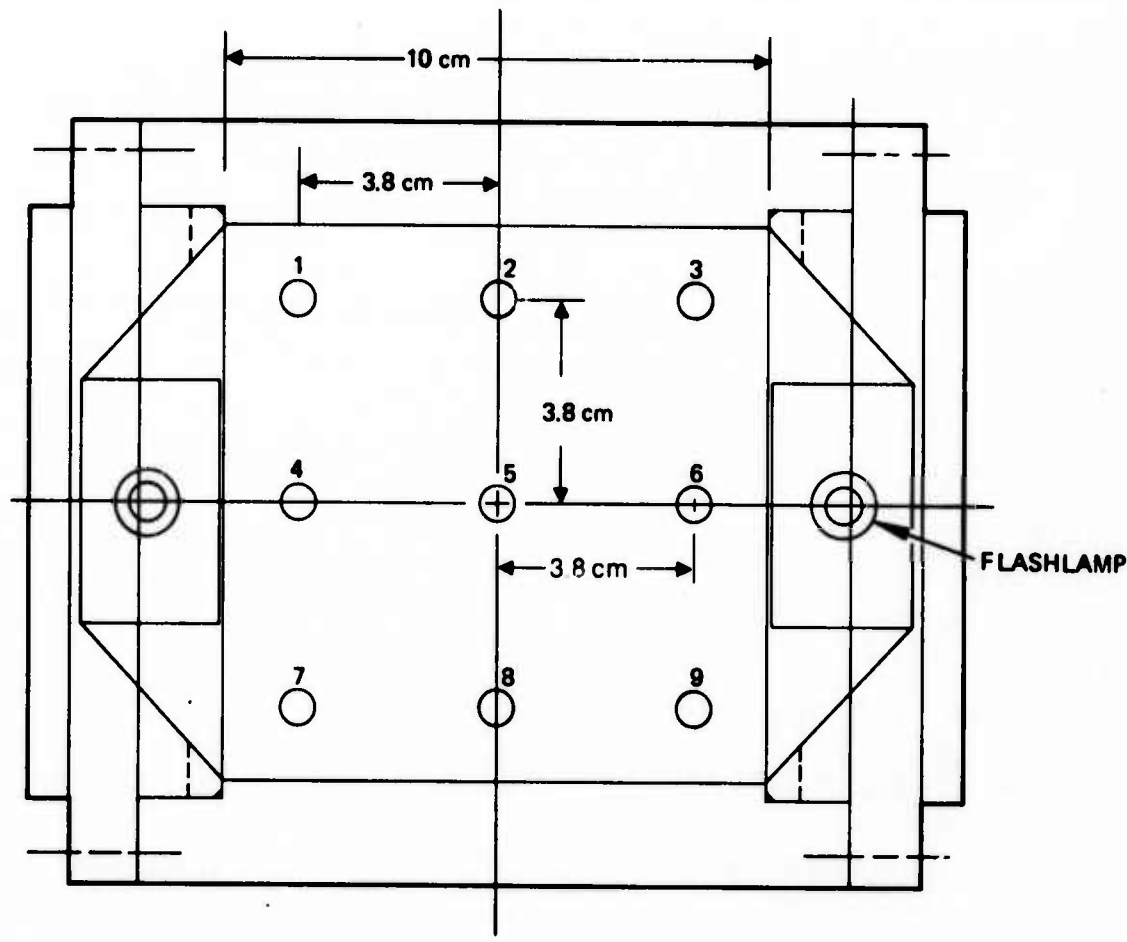


Fig. IV-2. Diagram showing window locations used to measure small-signal beam in DF-CO₂ laser.

TABLE IV-1.
Experimental Conditions Used for Gain Measurements

mode control studies, while the above mixture ratio gives nearly optimum laser power extraction (mixture ratios with larger amounts of F_2 such as 3:1:1:5:10 produced higher gain and more laser power for a given flashlamp initiation, however, for this study the amount of increase did not warrant the increased consumption of fluorine).

An oscilloscope trace of the gain profile for location 1, 3, 7, or 9, along with the flashlamp temporal profile for a $F_2:D_2:CO_2:He = 1.5:1:5:10$ mixture at a total pressure of 200 Torr is shown in Fig. IV-3. The gain pulse (lower trace) begins to rise near the peak of the flashlamp output (upper trace) and peaks approximately 30 μs later. The gain falls monotonically for approximately 34 μs after reaching its peak and then begins to randomly oscillate before becoming negative. This random oscillation is caused by a detonation wave traveling outward from the flashlamps. The pressure and temperature gradients in the wake of the wave cause severe medium inhomogeneities which steer the probe beam across the detector. The spatial and temporal behavior of these detonation waves will be discussed in more detail when the results of the holographic interferometric measurements are given in Section IV-B.

In Fig. IV-4 we have plotted the small-signal gain for two different flashlamp input energies, 1.7 and 1.07 kJ. In both cases the mixture ratio and total cavity pressure are the same, $F_2:D_2:CO_2:He = 1.5:1:5:10$ and 200 Torr, respectively. The gain profiles are given at four locations covering one quarter of the laser cavity. In both cases the largest measured gain occurs nearest the flashlamp (location 6) as would be expected since initiation of the chemical reaction is strongest in this region. For an input energy of 1.7 kJ, the peak gain at cavity center (location 5) is 2.6 %/cm or 22 dB per roundtrip. Nearest the flashlamp (location 6) the peak gain is 3.1 %/cm, higher by approximately 18% from location 5. The peak gain at locations 8 and 9 are nearly the same and are somewhat lower than at cavity center.

3569-7

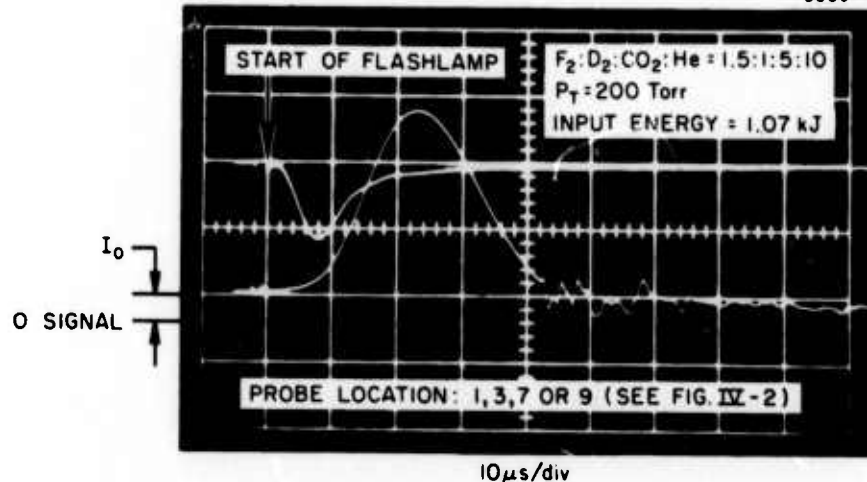
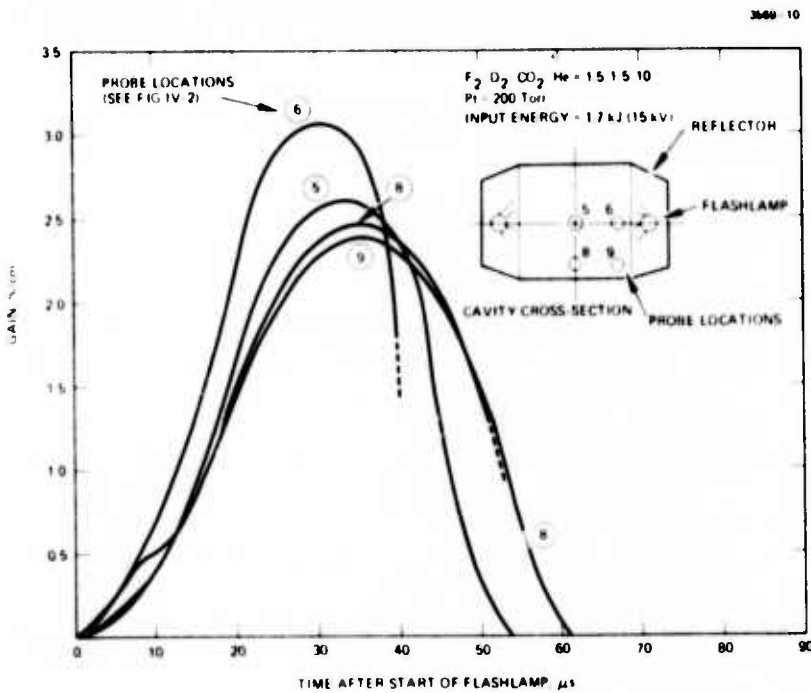
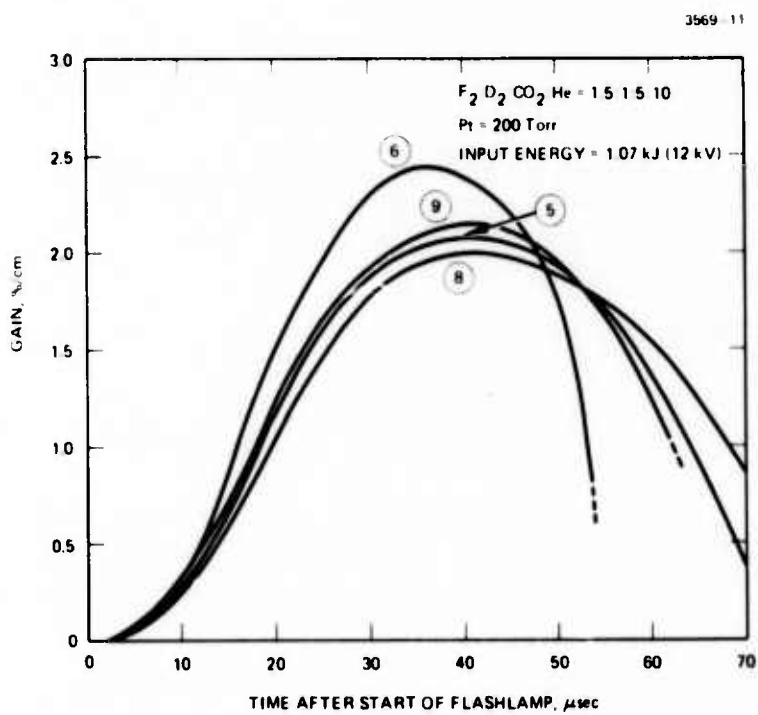


Fig. IV-3. Oscilloscope traces of gain and flashlamp profiles; upper trace - flashlamp, lower trace - gain profile. Peak small-signal gain is 2.1%/cm. Flashlamp discharge energy, 1.07 kJ (15 μF, 12 kV).



(a) Input energy = 1.7 kJ

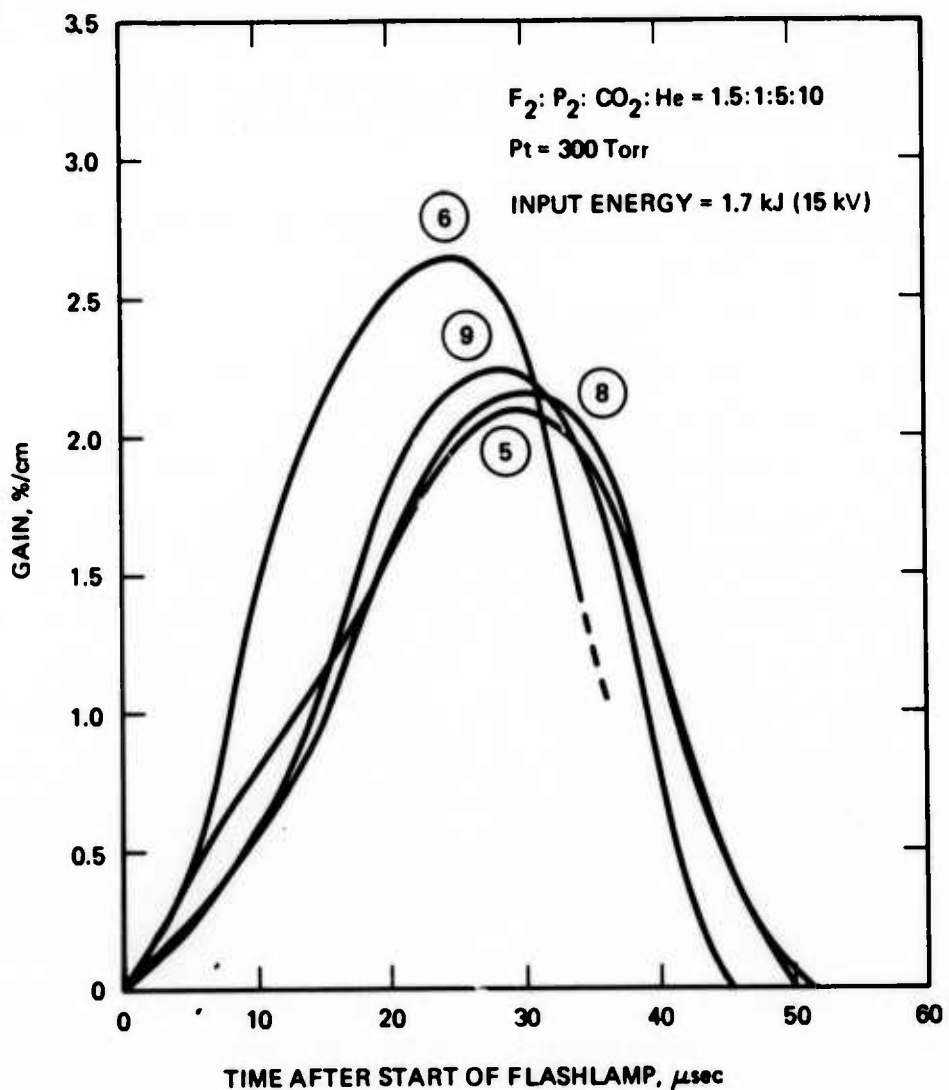


(b) Input energy = 1.07 kJ

Fig. IV-4. Axial small-signal gain for four transverse locations in a flash photolysis $DF-CO_2$ laser. 36

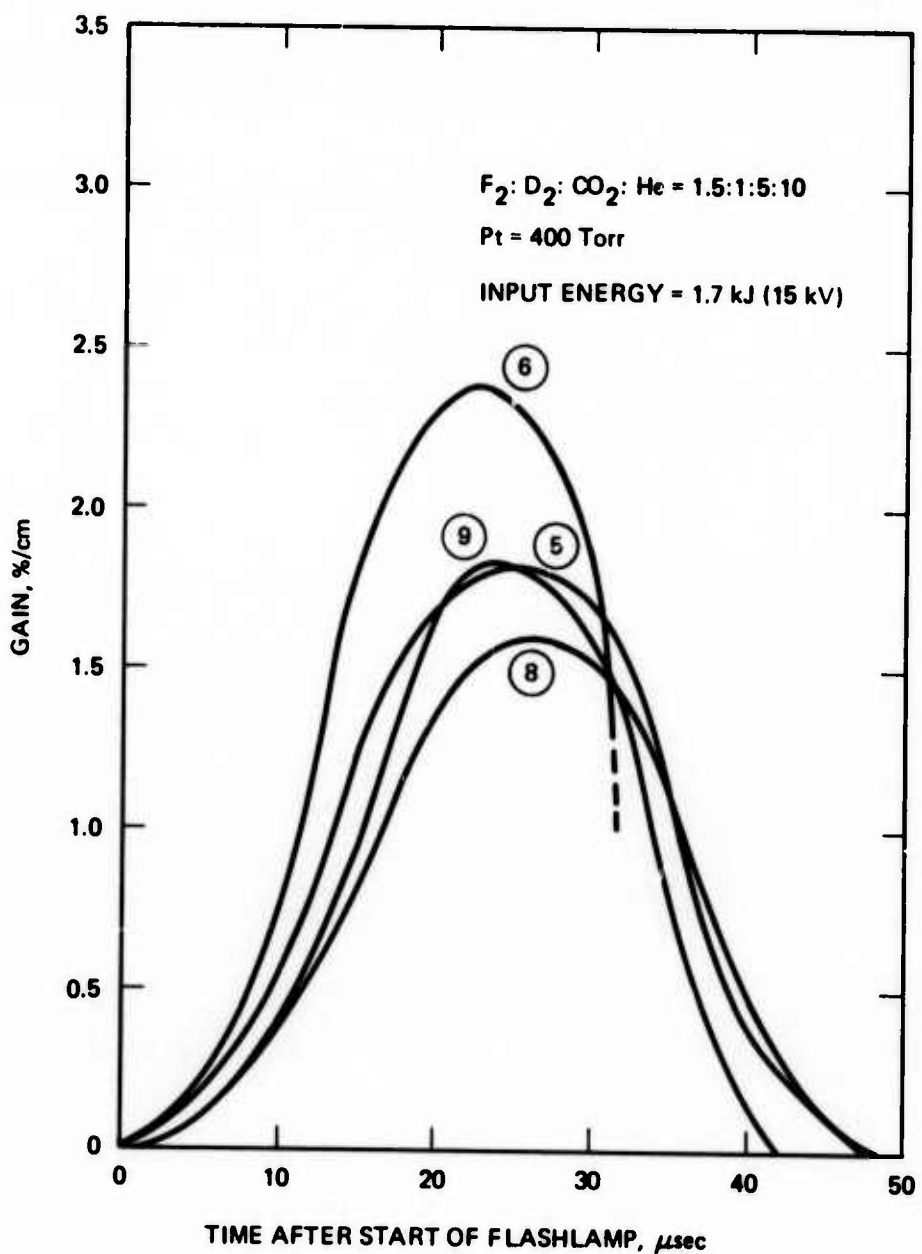
Because the chemical reactions at location 6 proceed faster than at the other locations, the gain at this location will rise faster, peak at a higher value, and fall to zero or negative sooner than location further from the flashlamps. If we use a 7.5 cm square resonator to cover the laser medium, and assumed an oscillating threshold of 0.5%/cm, the center of the resonator would have sufficient gain out to nearly 50 μ s, while the medium at the outer edges of the resonator nearest the flashlamp becomes spatially very nonuniform (indicated on the curves by a dashed line) and becomes absorptive before 40 μ s. We can delay the arrival of the detonation wave by decreasing the input energy as is shown in Fig. IV-4(b). Decreasing the input energy slows the chemical reaction near the flashlamps, causing a delay in the initiation of the detonation wave. By lowering the input energy to 1.07 kJ, the arrival of the wave is delayed approximately 14 μ s; permitting a longer period of active gain in an undisturbed medium. We found that decreasing the input energy to 0.75 kJ delays the arrival of the wave at location 6 until the gain becomes negative. The tradeoff that must be made, however, when lowering the input energy is reduced overall gain. The peak gain at cavity center decreases from 2.6%/cm to 2.1%/cm when the input energy is lowered from 1.7 kJ to 1.07 kJ. Decreasing the input energy to 0.75 kJ, lowers the gain to 1.5%/cm. Decreasing the input energy increases the useful time period of active gain, but does not greatly improve spatial gain uniformity. We can control the amount of nonuniformity by using resonators that are located in the center of the cavity and have outer diameters less than approximately 4 cm. Using this procedure, we should be able to maintain gain uniformity to within $\pm 5\%$ except for the extreme tail of the active gain curve where the gain falls through oscillating threshold.

In Fig. IV-5 we have plotted the gain curves for a total cavity pressure of 300 Torr and 400 Torr, respectively. The overall profile for both pressures is similar to the ones at 200 Torr. The basic differences are less gain and shorter gain pulse lengths for the higher pressures. Since it is desirable in most of our mode control studies to



(a) Total pressure = 300 Torr.

Fig. IV-5. Axial small-signal gain for four transverse locations in a flash photolysis DF-CO₂ laser.



(b) Total pressure = 400 Torr.

Fig. 5. Axial small-signal gain for four transverse locations in a flash photolysis $DF-CO_2$ laser.

obtain good medium uniformity while being able to obtain large gains, it does not appear that pressures above 200 Torr are advantageous.

The reader should note that the position and peak values of the gain profiles at locations 5, 8, and 9 do not have a fixed relationship for the conditions presented on Figs. IV-4 and IV-5. It is our belief that the gain profiles at these locations should be nearly identical for these conditions. Since the experimental data necessary to generate these curves are not taken simultaneously, changes in experimental conditions vary slightly from run to run causing some inconsistency. Because the amount of discrepancy is small, we did not feel that further investigation for the mode control studies was warranted.

B. Medium Homogeneity

1. Experimental Technique

Medium homogeneity measurements were made using double-exposure pulsed holographic interferograms. For this technique, one of the exposures of the hologram (in our case it was always the second one) was taken during empty cavity conditions, and the other exposure at some specific time during the chemical reaction. The double exposed film, after being properly developed, was then illuminated by a cw He-Ne laser, and the resulting interference fringes recorded on polaroid film.

The advantages of the holographic technique over standard interferometric techniques (e.g., a Mach-Zehnder interferometer) are ease of alignment and reduced optical quality requirements for the components of the interferometer. Standard interferometers require that the two interfering beams be aligned exactly parallel, and that the optical quality of the components used to either reflect or transmit the two beams be good to fractions of a wavelength. Holographic interferometers, on the other hand, can operate with angles in excess of 20° between the two interfering beams, and because two exposures are made, all fixed beam distortions such as those caused by poor window or mirror quality are cancelled and do not appear in the reconstructed holograms. The only optical component in the holographic interferometer that must be of high

quality is the optical wedge which is inserted during one of the film exposures. The wedge is used to produce a background set of parallel, evenly spaced fringes in the reconstructed holograms. For laser cavity disturbances having optical phase shifts on the same order as the optical wedge, the resulting deformed fringe pattern can be used to interpret the magnitude and spatial distribution of the axially integrated medium disturbances.

Figure IV-6 shows schematically the experimental arrangement used. The ruby laser was Q-switched by means of a Pockels-cell and produced 25 ns output pulses with a peak power of 1 MW. The output beam was made to operate on a single transverse mode by using a 2-mm diameter aperture located inside the optical cavity, and an etalon was used for single longitudinal mode selection. The beam from the ruby laser is directed into two nearly equal intensity beams that will be referred to as the object and reference beams. The object beam is sent through a Gland-type prism polarizer, expanded and collimated at a diameter of 13 cm, passed through an optical wedge with 53 s of arc (this gives approximately 4.5 fringes/in. at the film surface), passed through the DF-CO₂ laser cavity with ordinary plate glass for windows, and is incident on the recording film.

The holograms were recorded on Kodak SO173 film or 120-02 plates with a resolution of 1200 lines/mm. The best signal to noise ratio was determined experimentally and was found to occur when the intensity of the reference beam was approximately 3 times that of the object beam. The transparency of the developed holograms was too small to obtain adequate transmitted light for reconstruction. This was caused by the film being overexposed by the radiation from the flashlamps in the DF-CO₂ laser cavity. Placing Wrattan filters in front of the film to attenuate wavelengths below 6943 Å proved unsuccessful in noticeably improving the transparency. We were able, however, to solve the transparency problem by bleaching the holograms in bromine vapor after the film had been developed and fixed. This procedure converts all the silver in the film emulsion to silver bromide which is transparent at visible wavelengths. In doing this, reconstruction occurs due to a phase rather than amplitude grating effects.

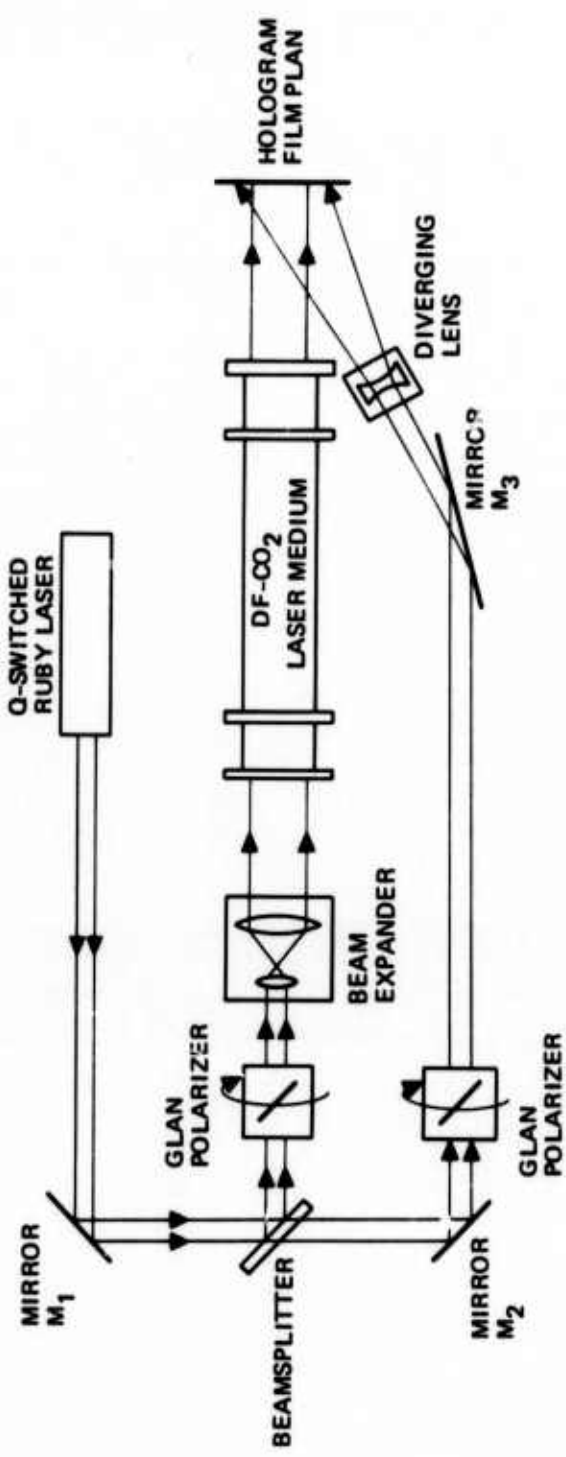


Fig. IV-6. Holographic experimental set-up.

The change from an amplitude to a phase hologram does not change the reconstruction procedure which uses a He-Ne laser. The output beam from the laser is sent through a negative lens identical to the one in the reference beam, and made to illuminate the film in a nearly identical manner as does the reference beam during construction of the hologram. When the holograms are properly reconstructed, their virtual images are nondiverging.

In preparation for making holograms of the laser medium, the output beam of the ruby laser was checked for transverse mode uniformity and checked for alignment throughout the optical train. Once proper alignment was assured, the entire optical path for the object and reference beams was enclosed to minimize the effect of room air turbulence on the experimental data. A delay time that controls the firing sequence of the flashlamps and the Pockels-cell was chosen and preset. The delay unit receives an input signal from the DF-CO₂ trigger control unit when both window shutters have fully opened. Once the input signal is received, the Pockels-cell fires exactly 1 ms later. Prior to the firing of the Pockels-cell the delay trigger which has a variable delay of 0 to 1 ms after receiving the input trigger, fires the flashlamps of the DF-CO₂ laser. Thus, a 1 ms delay setting produces a hologram at the beginning of the flashlamp initiation, while a 0.95 ms delay setting produces a hologram 50 μ s into the initiation. After selecting the desired delay time, the DF-CO₂ laser window shutters were closed, the flashlamp capacitors charged, and the cavity filled with the desired gas mixture and pressure. The optical wedge was placed in the object beam, and the firebutton depressed to open the shutters and start the firing sequence. After the first film exposure, the optical wedge was removed and two minutes were allowed to elapse before the ruby was fired for the second time, giving the second exposure for empty cavity conditions. We found that this procedure gave repeatable results.

In the following section we will present polaroid pictures of reconstructed holograms taken at different laser cavity conditions.

2. Experimental Results

In this section the spatial and temporal medium density properties of the DF-CO₂ laser are presented. Again, as we did in making gain measurements, only one-quarter of the laser cavity was probed. Figure IV-7 shows the exact dimensions and location of the window located at each end of the laser cavity. The window is 5-cm square and is offset slightly from the lower corner to allow some coverage of the cavity center.

A typical photograph showing the fringes obtained prior to onset of the chemical reaction is given in Fig. IV-8. From the fringe spacing and their uniformity we can show that the medium optical uniformity is better than $\lambda/15$ at 10.6 μm across the entire 5-cm aperture. Our first attempts to obtain this degree of medium uniformity were unsuccessful until we more closely matched the atomic weight of the gases in the window purge region and the laser cavity. Initially, we used pure argon (atomic weight = 40) in the window purge region and a F₂:D₂:CO₂:He = 1.5:1:5:10 mixture (average atomic weight = 19.5) in the laser cavity. We found that small pressure differences between the cavity and the purge region would cause the heavier argon gas to fold over on the lighter cavity gas when the shutters were opened causing a fairly significant gas density inhomogeneity. A photograph of the interferometric hologram obtained with pure argon in the purge region is shown in Fig. IV-9. Note that the gas near the bottom of the cavity is relatively undisturbed while the gas above this region shows an increasingly higher density. From the tilt of the fringes, the optical phase shift between the top and bottom of the resonator is determined to be nearly $\lambda/2$ at 10.6 μm . By adding helium to the argon in the window purge region, we were able to more closely match the atomic weights and obtain results similar to those in Fig. IV-8.

The photographs in Figs. IV-10 through IV-12 show the holograms obtained for a F₂:D₂:CO₂:He = 1.5:1:5:10 mixture at 200 Torr and a total flashlamp input energy of 1.7 kJ. The holograms were taken at 10, 21, 30, 41, and 50, and 61 μs after the start of the flashlamps.

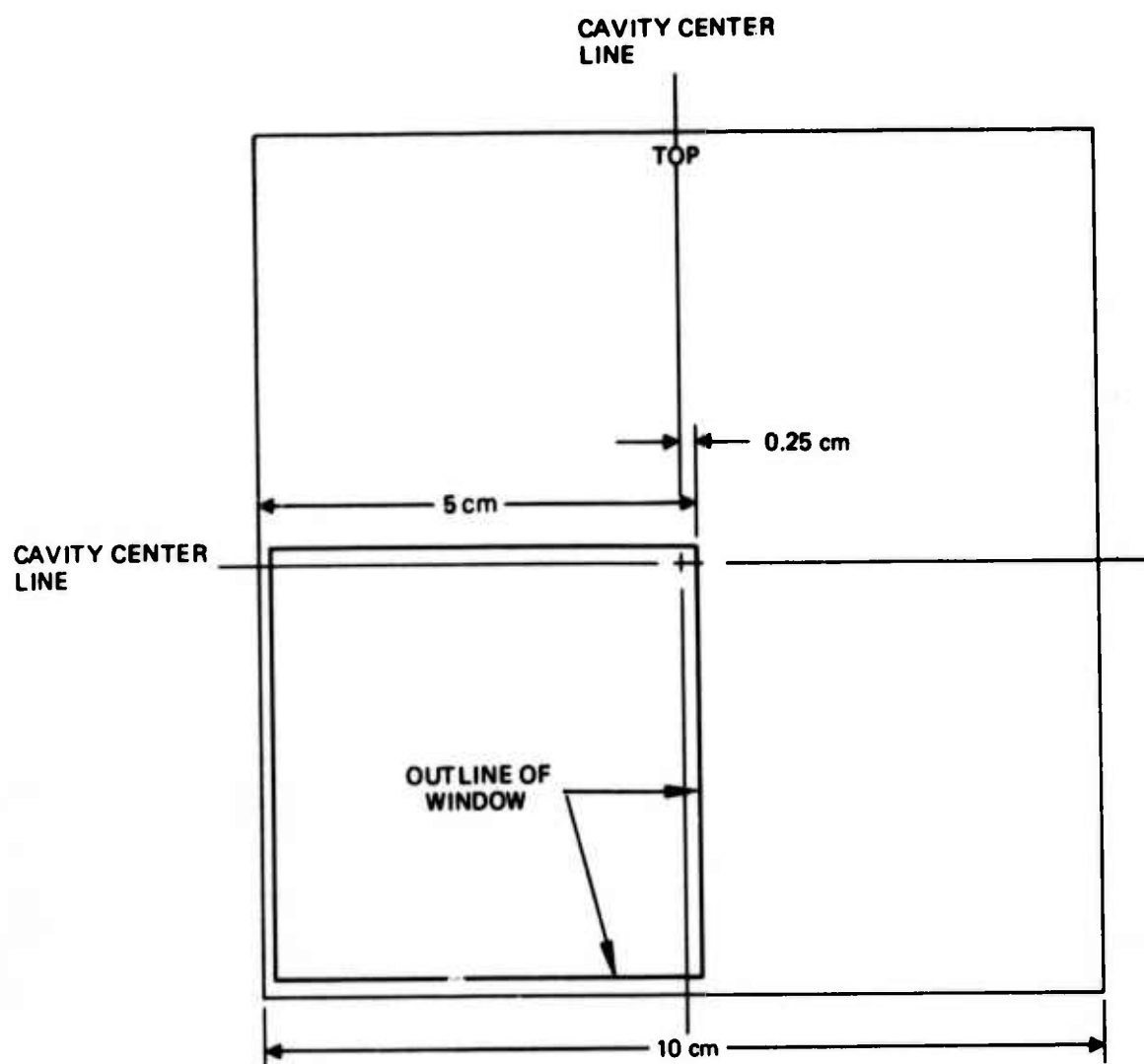


Fig. IV-7. Diagram showing window location used to measure medium homogeneity in DF-CO₂ laser.

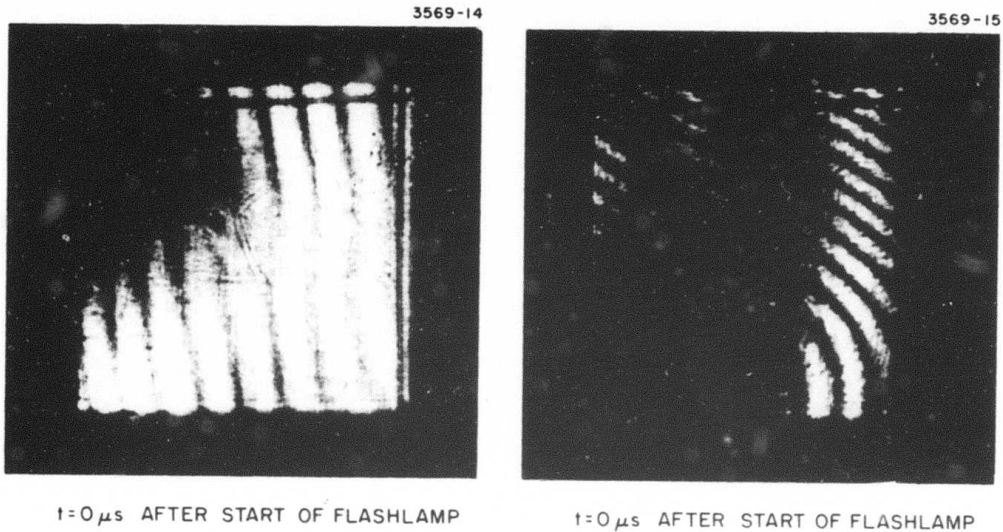
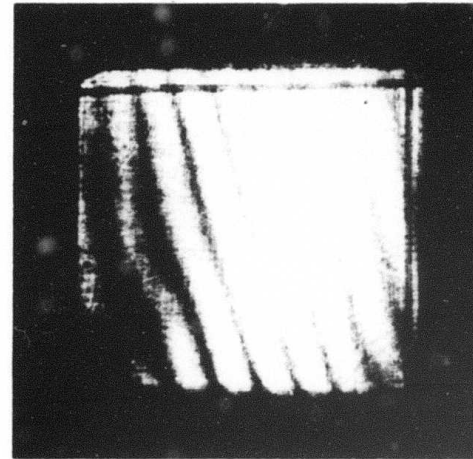


Fig. IV-8.
Hologram for $\text{F}_2:\text{D}_2:\text{CO}_2:\text{He} = 1.5:1:5:10$ mixture at 200 Torr, $t = 0 \mu\text{s}$, Ar/He window purge.

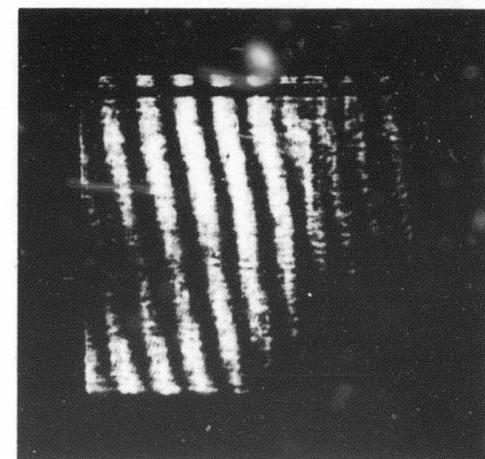
Fig. IV-9.
Hologram for $\text{F}_2:\text{D}_2:\text{CO}_2:\text{He} = 1.5:1:5:10$ mixture at 200 Torr, $t = 0 \mu\text{s}$, Ar window purge.

3569-16



a. $t=0\ \mu\text{s}$ AFTER START OF FLASHLAMP

3569-17



b. $t=21\ \mu\text{s}$

Fig. IV-10. Holograms for $\text{F}_2:\text{D}_2:\text{CO}_2:\text{He} = 1.5:1:5:10$ mixture at 200 Torr, for $t = 0$ and $20\ \mu\text{s}$ after start of flashlamp (input energy = 1.7 kJ).

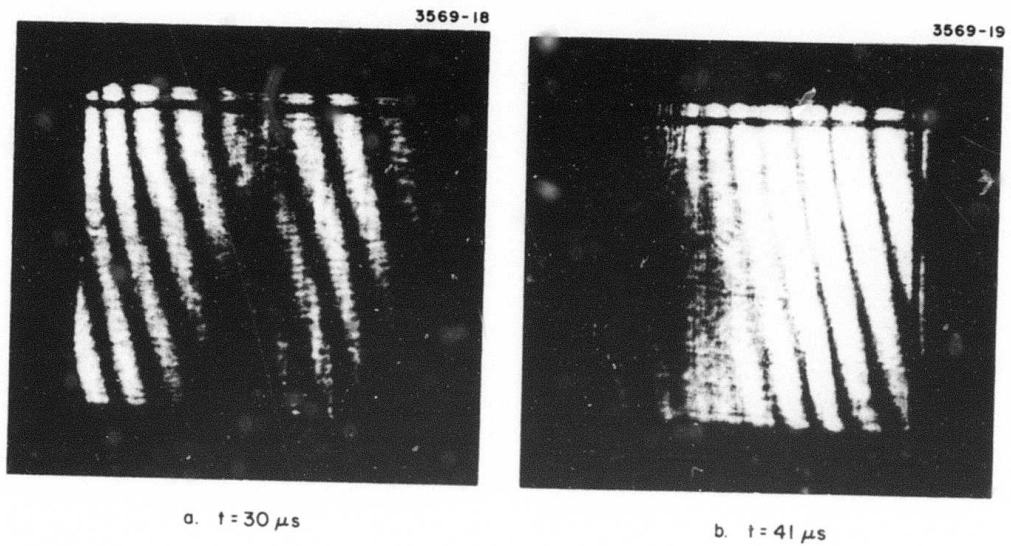


Fig. IV-11. Holograms for $F_2:D_2:CO_2:He = 1.5:1:5:10$ mixture at 200 Torr, for $t = 30$ and $41 \mu s$ after start of flashlamps (input energy = 1.7 kJ).

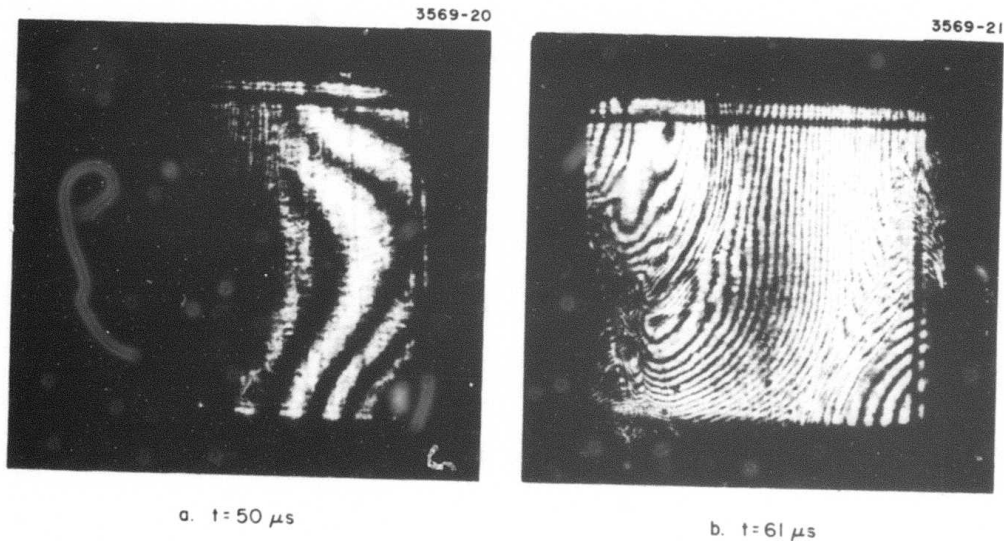


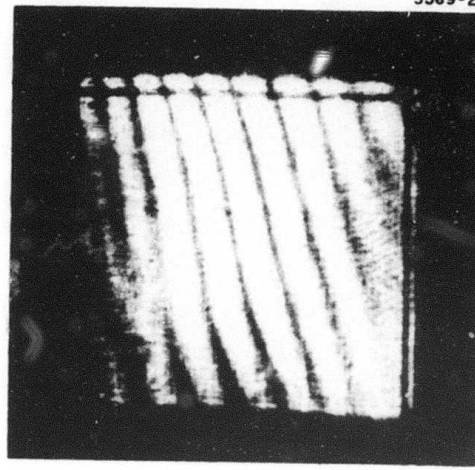
Fig. 12. Holograms for $F_2:D_2:CO :He = 1.5:1:5:10$ mixture at 200 Torr, for $t = 60$ and $71 \mu s$ after start of flashlamps (input energy = 1.7 kJ).

For times approaching 40 μ s, the medium uniformity across the entire window aperture is better than $\lambda/9$. For times greater than approximately 40 μ s, an increasingly larger percentage of the cavity becomes perturbed by a detonation wave emanating from the flashlamps. The detonation wave is generated at the flashlamp envelope where the chemical reaction is strongly initiated. The wave propagates outward continuously supporting itself with the F_2 and D_2 in its path. By $t = 41 \mu$ s, the outer edge of the cylindrically shaped wave has progressed approximately 1.2 cm along a line connecting the flashlamps. This distance corresponds to the gain probe locations 4 or 6 in Fig. IV-2, and verifies the source of the random oscillations (note dashed line for probe location 6 occurring at 41 μ s in Fig. IV-4) in the detector signal during gain measurements. In Fig. IV-10(b) we see that the detonation waves from the left and right flashlamps have intersected at the center of the cavity.

We can determine the speed of the detonation waves from Figs. IV-11(a) and IV-12(a) by taking the ratio of the distance covered by the waves between $t = 41$ and 50μ s, and the time differential of 9 μ s. This procedure gives a velocity of 1.7×10^5 cm/s. For this mixture and a temperature of 450^0 K the sound speed is calculated to be approximately 550 m/s; indicating a supersonic mach number of 3.1 for the detonation wave.

Photographs in Figs. IV-13 and IV-14 show the holograms obtained using a lower input energy (0.75 kJ). As we pointed out in Section III-A, the arrival of the detonation wave in the cavity can be delayed by decreasing the input energy to the flashlamps. This is verified from the photographs by noticing that the medium density uniformly is maintained at greater than $\lambda/10$ for times approaching 70 μ s (this is compared to 40 μ s for input energies of 1.7 kJ). At 70 μ s a disturbance typical of an acoustic wave (probably generated by local flashlamp heating) appears; followed by the detonation wave at 80 μ s. Additional holograms are presented in Figs. IV-15 and IV-16 for a cavity pressure of 300 Torr and an input energy of 1.7 kJ. The results are similar to those already presented, the medium remains essentially

3569-22

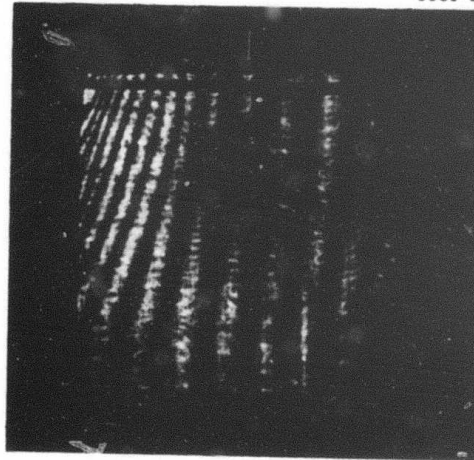
a. $t = 41 \mu\text{s}$ AFTER START OF FLASHLAMP

3569-23

b. $t = 61 \mu\text{s}$

Fig. IV-13. Interferometric holograms for $\text{F}_2:\text{D}_2:\text{CO}_2:\text{He} = 1.5:1:5:10$ mixture at 200 Torr, for $t = 41$ and $61 \mu\text{s}$ (input energy = 0.75 kJ).

3569-24

a. $t = 70 \mu\text{s}$ AFTER START OF FLASHLAMP

3569-25

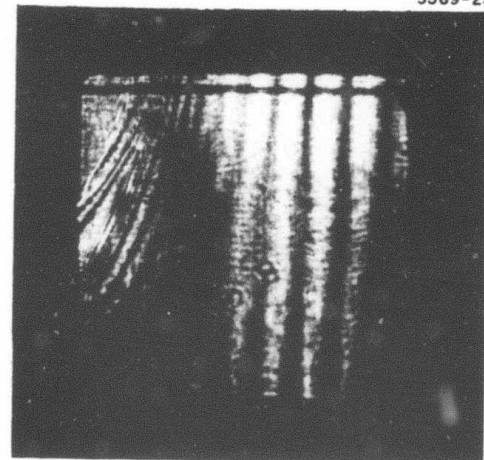
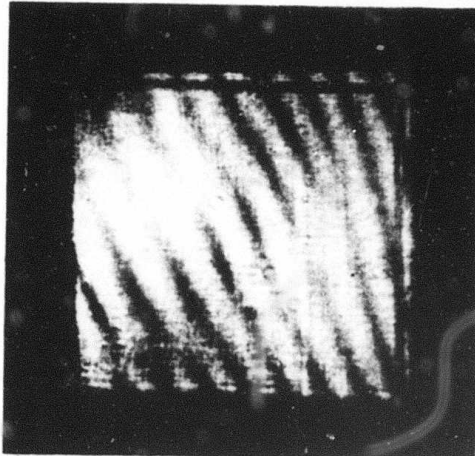
b. $t = 81 \mu\text{s}$

Fig. IV-14. Interferometric holograms for $\text{F}_2:\text{D}_2:\text{CO}_2:\text{He} = 1.5:1:5:10$ mixture at 200 Torr, for $t = 70$ and $81 \mu\text{s}$ (input energy = 0.75 kJ).

3569-26

a. $t = 21 \mu\text{s}$ AFTER START OF FLASHLAMP

3569-27

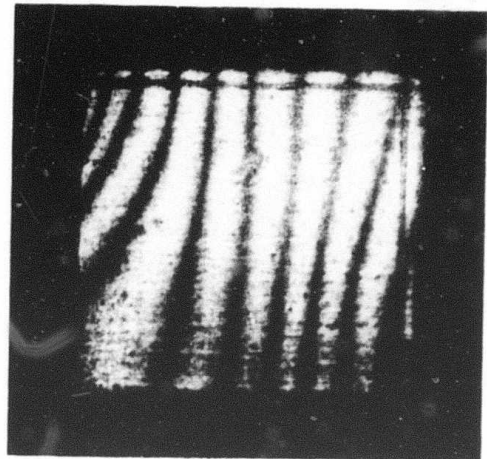
b. $t = 30 \mu\text{s}$

Fig. IV-15. Interferometric holograms for $\text{F}_2:\text{D}_2:\text{CO}_2:\text{He} = 1.5:1:5:10$ mixture at 300 Torr, for $t = 21$ and $30 \mu\text{s}$ (input energy = 1.7 kJ).

3569-28

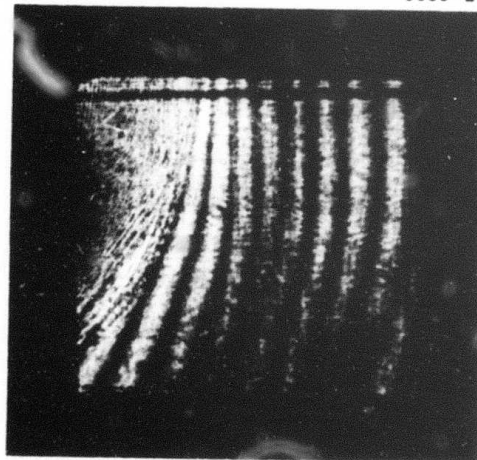
 $t = 41 \mu\text{s}$ AFTER START OF FLASHLAMP

Fig. IV-16.
Interferometric holograms
for $\text{F}_2:\text{D}_2:\text{CO}_2:\text{He} = 1.5:1:5:10$ mixture at 300 Torr, for
 $t = 41 \mu\text{s}$ (input energy = 1.7 kJ).

uniform until the passage of a detonation wave. The higher pressure results show the detonation wave to be considerably stronger and arriving in the cavity approximately 3 μ s earlier.

From the results presented here we can conclude for our mode control studies that the laser medium will remain uniform to $\lambda/9$ or better prior to the passage of an acoustic or detonation wave. The supersonic detonation wave, which is the most detrimental to optical beam quality, can be delayed significantly by reducing the flashlamp input energy or to a smaller degree by reducing the cavity pressure. For future mode control studies or any laser operation where good beam quality is desired, we can avoid these disturbances by removing the flashlamp from the reactive mixture. In doing this, we eliminate the rapid chemical reaction in the immediate vicinity of the flashlamps; thereby eliminating the detonation waves. For the present study, however, we will reduce the effect of the disturbances on the resonator by using input energies of 1.07 kJ or less and resonator mirror diameters of 4 cm or less. The latter procedure places the outer edges of the resonator near the cavity center; therefore avoiding the waves until essentially the end of the laser pulse.

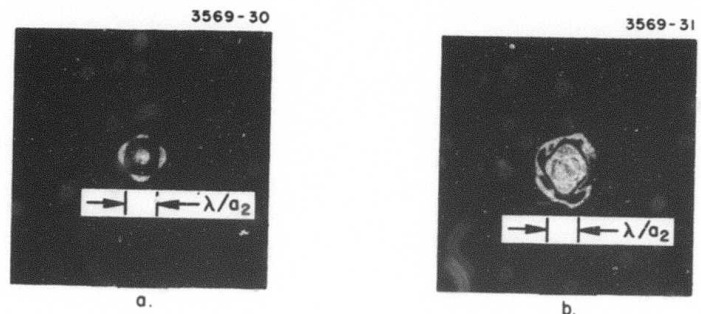
V. EXPERIMENTAL AND THEORETICAL RESULTS

A. Beam Quality Measurements

Typical far-field patterns for the 77% output coupled resonators are shown in Fig. V-1. The patterns were made on developed polaroid film that was not exposed, and which had an ablation threshold of approximately 0.05 J/cm^2 . This threshold provided sufficient sensitivity to obtain adequate visible recordings of the far-field pattern. Ablation and visible changes in the density of the film surface are, however, extremely nonlinear and cannot be used as quantitative indicators of far-field beam quality.

The far-field pattern in Fig. V-1(a) was obtained for resonator configuration $N_{\text{eq}} = 2.1$, a cavity pressure of 200 Torr (all far-field beam quality information presented in this section was obtained with a cavity pressure of 200 Torr), and a flashlamp input energy of 0.7 kJ. The pattern shows a distinct central lobe surrounded by a single visible secondary lobe. The pattern in Fig. V-1(b) is for resonator configuration $N_{\text{eq}} = 2.5$, and a flashlamp input energy of 1.7 kJ. Note the overall pattern is similar to the above pattern except the null between the central and fast side lobe is not as well defined and the appearance of a second side lobe shows some smearing. The distortion effects are probably due to the detonation waves which reach the resonator before lasing is complete when an input energy of 1.7 kJ is used (see Section IV-B).

To obtain a more quantitative measure of the beam quality for the two resonators, we have compared the measured far field power transmitted through various apertures to values that would be obtained for a diffraction limited far-field beam. In Fig. V-2 for the $N_{\text{eq}} = 2.1$ resonator, and a flashlamp input energy of 0.7 kJ, the power in the central lobe (46%) is nearly equal to the power (51%) contained in the central lobe of a diffraction limited beam. The difference between the measured and theoretical power can be explained by the tapered near-field intensity distributions which exist in low Fresnel number



(a) $N_{eg} = 2.09$,
 flashlamp
 input energy =
 0.75 kJ.

(b) $N_{eg} = 2.5$,
 flashlamp
 input energy =
 1.7 kJ.

Fig. V-1. Far-field mode patterns for unstable resonator with geometric magnification $M = 2.1$.

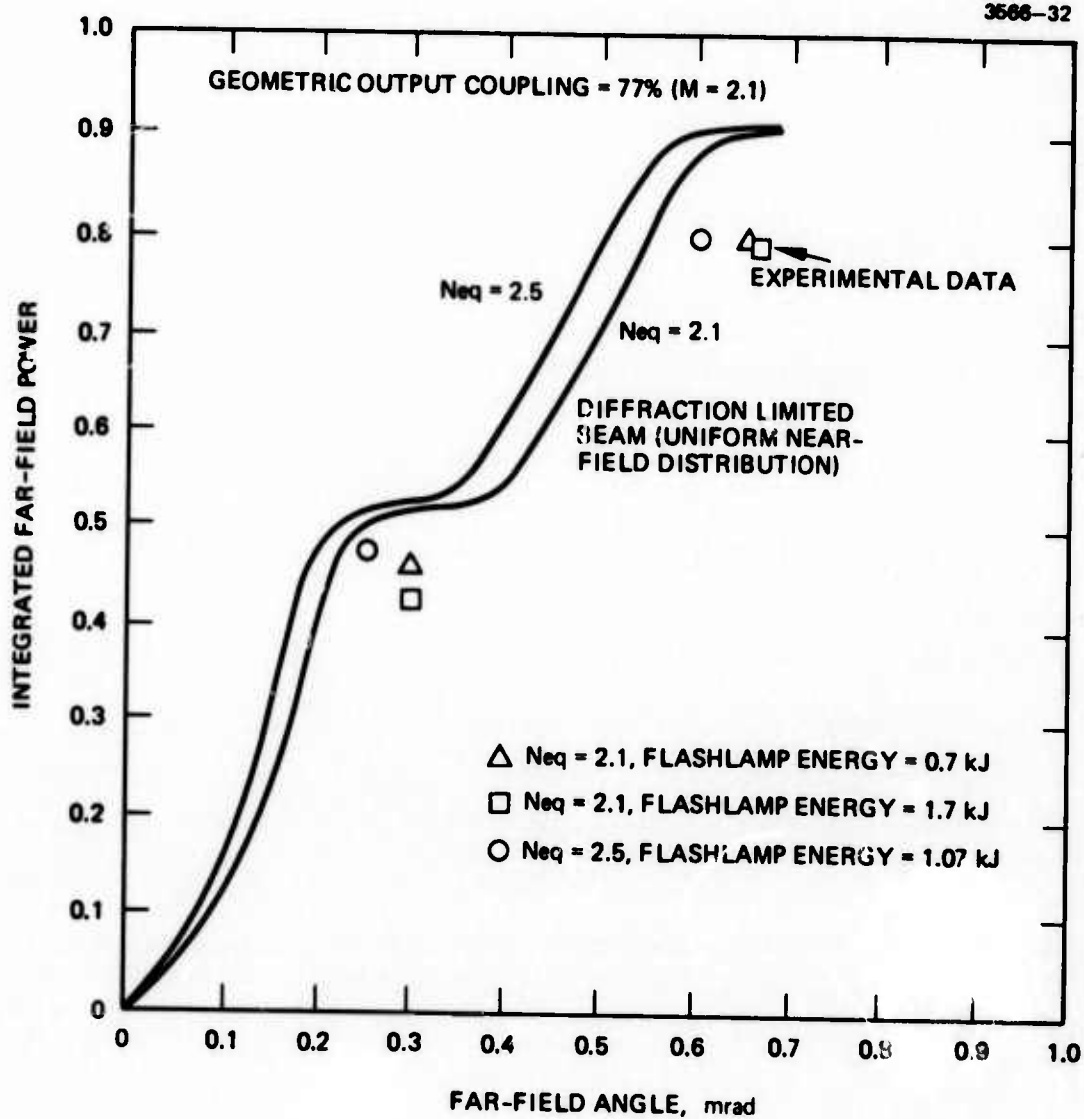


Fig. V-2. Comparison of measured and ideal integrated far-field power for confocal unstable resonator, $M = 2.1$, $N_{eq} = 2.1$ and 2.5 .

resonators. In Section V-B we show that the nonperturbed fundamental transverse mode, calculated using our resonator computer program, produces approximately 47% of the far-field power in the central lobe. In Fig. V-2 the amount of power contained in the central lobe for the $N_{eq} = 2.5$ resonator is 48%, and is nearly equal to the ideal power of 52%. When we include the power contained in the first secondary lobe, we see that for the two resonators the transmitted power is nearly identical. Increasing the flashlamp input energy decreases the central lobe power of the $N_{eq} = 2.1$ resonator from 46% to 43%. This is consistent with the far-field patterns in Fig. V-1. The experimental data points given in the figure were found to be repeatable to within $\pm 5\%$.

We can conclude from the results in Fig. V-2 that the 77% ($M = 2.1$) loss coupled resonators shows no Fresnel number dependence on resonator beam quality.

Similar data for the 50% loss coupled resonators are shown in Fig. V-3. The experimental data was taken for resonators with $N_{eq} = 1.02$ and 1.4 (data was also taken for $N_{eq} = 1.6$ and was found to be similar to $N_{eq} = 1.4$). We can see that the measured results, when compared to the theoretical results, are nearly identical for the two resonators. Again, we can conclude that there is no dependence of beam quality on resonator Fresnel number.

Experimental data for the 30% loss coupled resonators are shown in Fig. V-4. The data was obtained for $N_{eq} = 1.2$ and 1.5. The experimental data is consistent with our previous results for the 50% and 77% loss coupled resonators in that no dependence on Fresnel number was found. A typical far-field pattern for resonator configuration $N_{eq} = 1.5$, $M = 1.2$ is shown in Fig. V-5. We can see that the far-field pattern has some distortion. As we mentioned earlier, low loss coupled unstable resonators are inherently sensitive to medium disturbances and mirror misalignment. In our laser system some misalignment often occurred because the resonator's mirrors were aligned under vacuum conditions. When the cavity was filled to a pressure of 200 Torr, the cavity structure would move, causing misalignment. Often the amount of misalignment could be predicted and

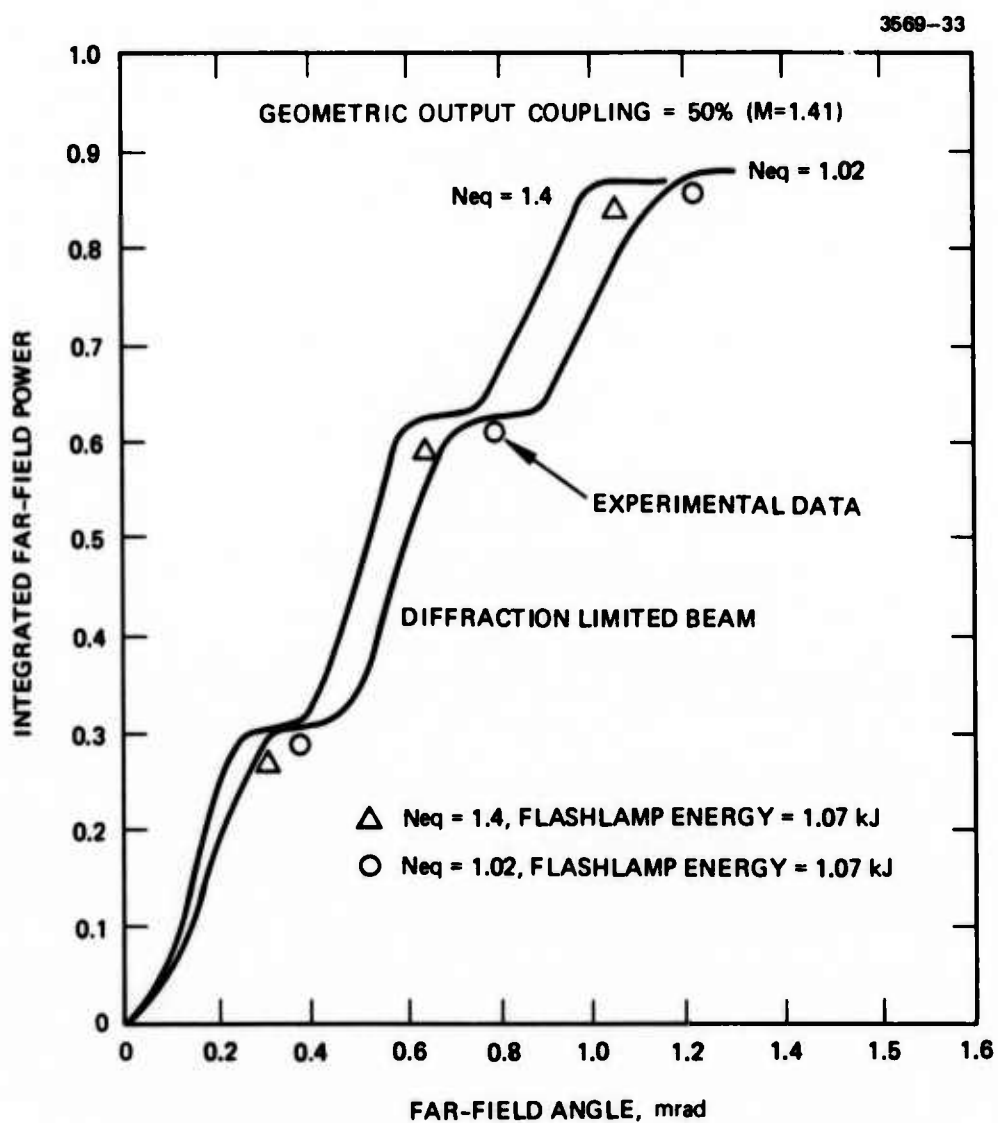


Fig. V-3. Comparison of measured and ideal integrated far-field power for confocal unstable resonator, $M = 1.41$, $N_{eq} = 1.02$ and 1.4.

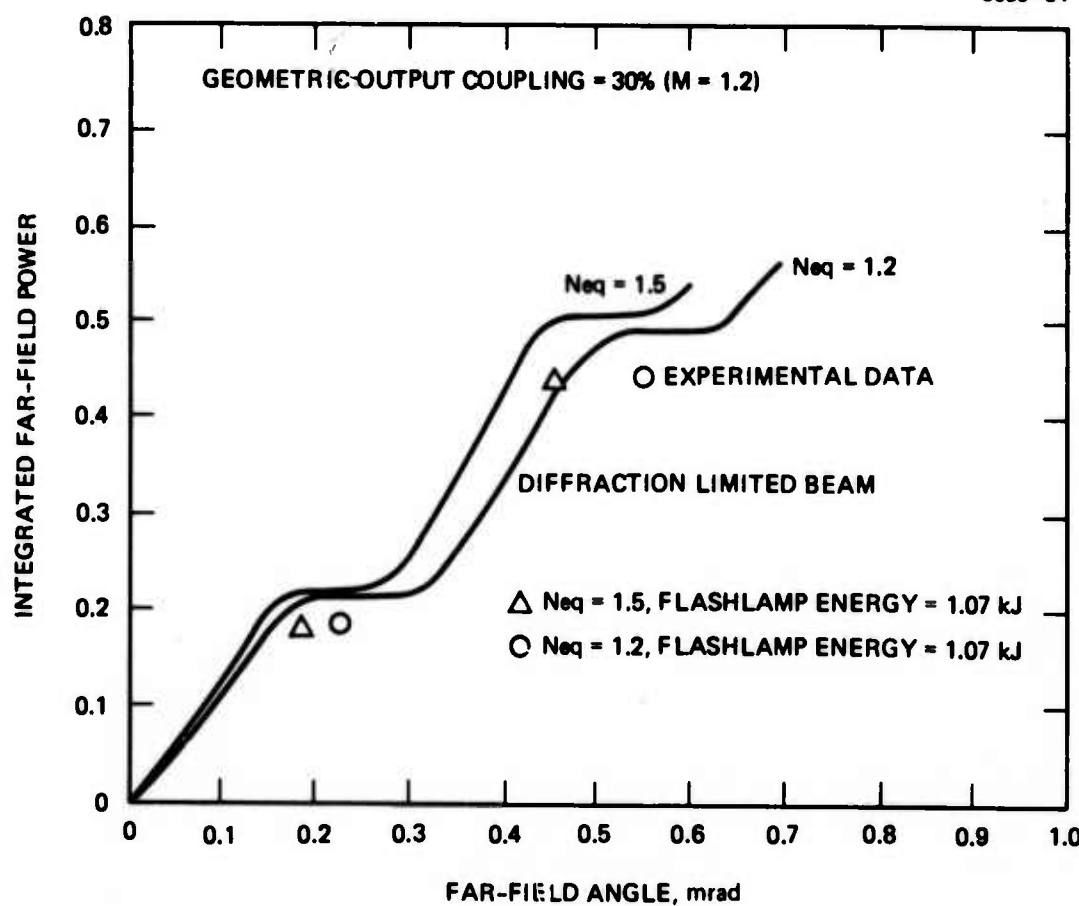


Fig. V-4. Comparison of measured and ideal integrated far-field power for confocal unstable resonator, $M = 1.2$, $N_{eq} = 1.2$ and 1.5 .

3569-35



Fig. V-5.
Far-field mode pattern for $N_{eq} = 1.5$,
 $M = 1.2$.

compensated for during alignment. At the higher loss couplings, the small amount of misalignment did not appreciably affect the far-field distribution.

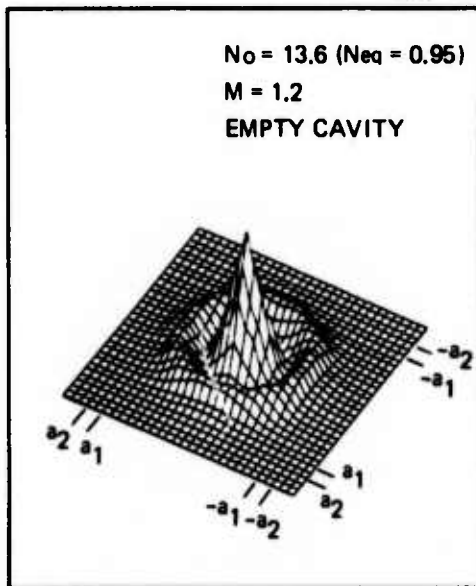
In order to determine if unstable resonators are likely to operate in a higher order mode with properties significantly different from those of the fundamental mode when phase perturbations exist in the cavity, we used the grooved mirror described in Section II as one of the resonator mirrors for the 30% and 77% loss coupled resonators. In the following sections we describe the analytical and experimental results of the perturbed resonators.

B. Resonator Calculations Using the Step-By-Step Propagation Algorithm

In order to obtain some indication as to what depth of grooves we should use for the phase perturbation studies, our 3-dimensional step-by-step resonator computer program⁽⁷⁻⁹⁾ was used to model the $N_{eq} = 0.95$, $M = 1.2$ and $N_{eq} = 2.5$, $M = 2.1$ unstable resonators. Details of the program have been well documented in the references indicated and will not be presented here. What will be presented are the physical dimensions of the resonators studied, any special considerations that were necessary in making the calculations, and specific results and conclusions.

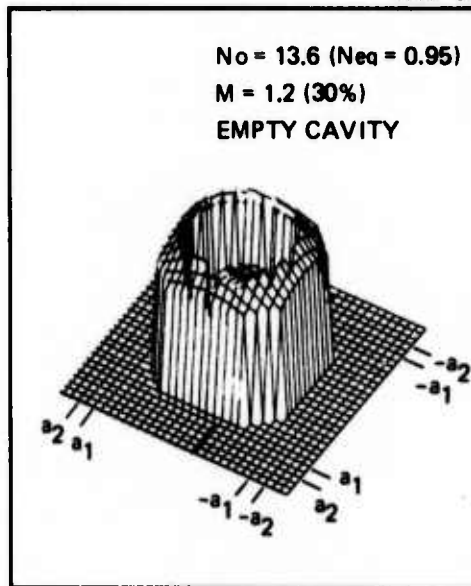
Table V-1 lists the parameters of the two resonators modeled. We first determined the intensity and phase distribution of the empty cavity mode, and the far-field intensity distribution for the output beam. The 3-dimensional profile plot for these distributions are given in Figs. V-6 and V-7 for the 30% ($M = 1.2$) and 77% ($M = 2.1$) coupled unstable resonators, respectively. The nonuniformity of the near field for the 30% coupled resonator shown in Fig. V-6(a) is expected because of the relatively low Fresnel number for the resonator. Note that for this configuration the field intensity has a null at a radial distance approximately equal to half the output mirror radius. The calculated output coupling is 9% compared to the geometric value of 30% because of the low intensity beyond the output mirror radius a . The near-field phase distribution is not uniform across the entire output aperture

3569-37



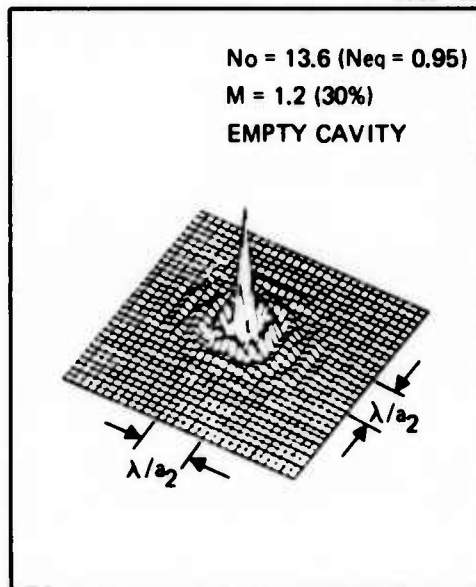
a. NEAR-FIELD INTENSITY

3569-38



b. NEAR-FIELD PHASE

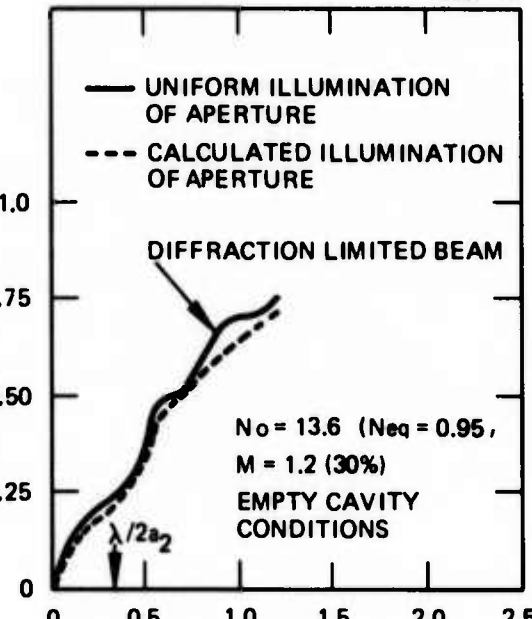
3569-39



c. FAR-FIELD INTENSITY

INTEGRATED FAR-FIELD INTENSITY

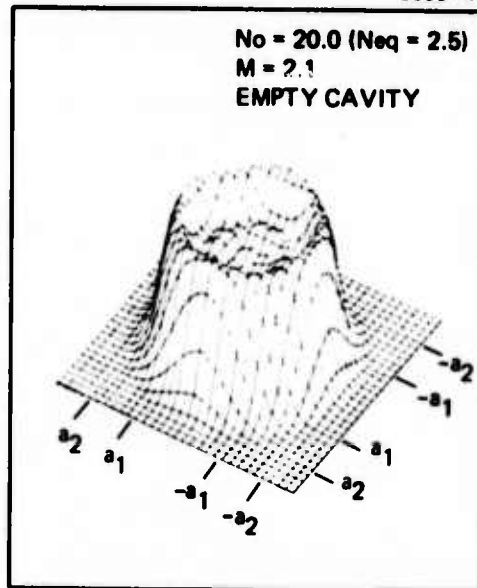
3569-40



d. FAR-FIELD ANGLE, mrad

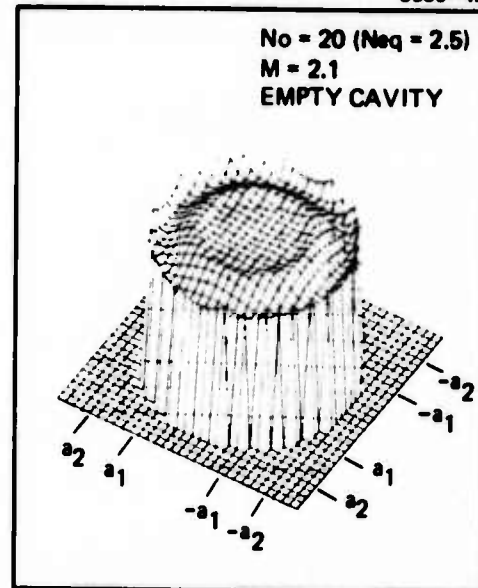
Fig. V-6. Calculated mode distribution for confocal unstable resonator $N_{eq} = 0.95$, $M = 1.2$ (empty cavity).

3569-41



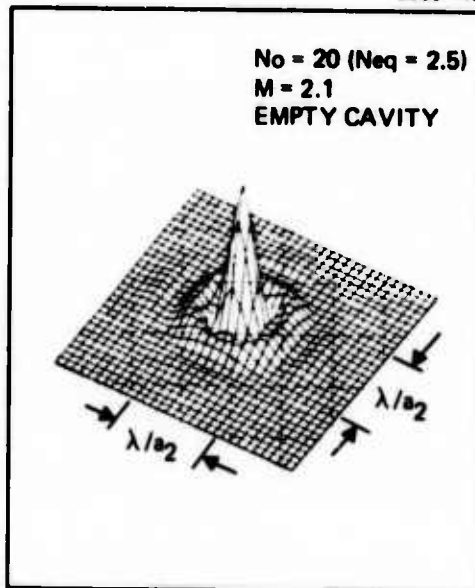
a. NEAR FIELD INTENSITY

3569-42



b. NEAR FIELD PHASE

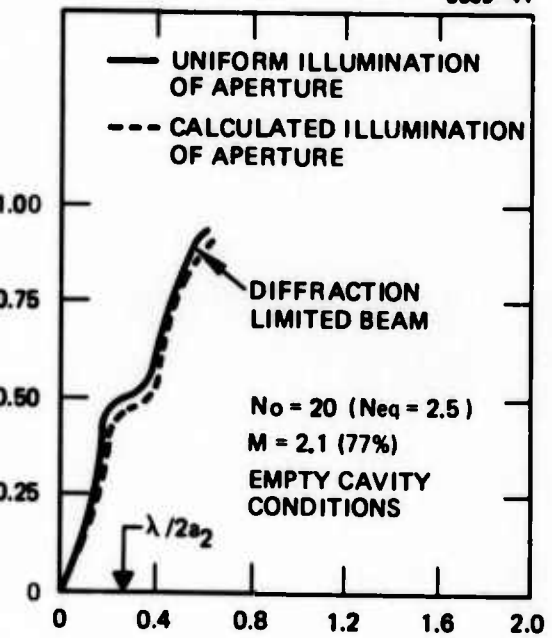
3569-43



c. FAR-FIELD INTENSITY

INTEGRATED FAR-FIELD INTENSITY

3569-44



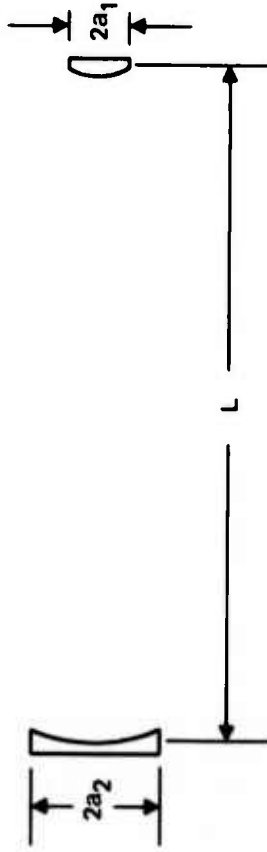
d. FAR-FIELD ANGLE, mrad

Fig. V-7. Calculated mode distribution for confocal unstable resonator $N_{eq} = 2.5$, $M = 2.1$ (empty cavity).

TABLE V-1.
Resonator Parameters Used in Computer Modeling

Resonator Parameters	30% Geometric Coupling	77% Geometric Coupling
$2a_2$ (cm)	3.24	3.91
$2a_1$ (cm)	2.70	1.86
L (cm)	180	180
Eq. Fresnel No.	0.95	2.5

3569-36



and has a positive radius of curvature characteristic of a converging beam. The phase plot is set to zero when the near-field amplitude drops to less than 7% of its peak. The phase at the center of the resonator is offset by π rad, with the base of the profile plot representing 0rad . The resulting far-field distribution is typical of low coupled unstabled resonators. The far field for these resonators has a central intensity lobe surrounded by several secondary lobes of decreasing intensity. From the curve in Fig. V-6(d) showing the integrated far-field power for the calculated results, we can see that only 18% and 40% of the total far-field power is contained in the central and first lobe, respectively. In comparing the calculated results with the ideal uniform illumination we see that the integrated intensity for the calculated results are somewhat lower but not significantly different from those predicted by geometric optics.

The near-field intensity distribution for the 77% coupled unstable resonator is considerably different from the distribution for the 30% coupled resonator shown in Fig. V-7(a). The near-field distribution occupies a larger percentage of the resonator and it does not have a low intensity null internal to the cavity. Because the Fresnel number of the resonator is still relatively low ($N_o = 20$), the near-field intensity distribution contains some structure. The distribution can be seen to peak just outside the output mirror and fall linearly to zero near the outer boundaries of the resonator. The near-field phase shows some structure with the maximum variation across the output aperture of 0.6 rad. The far-field distribution shows a central lobe with one significant side lobe. A comparison of the integrated far-field power shown in Fig. V-7(d) for the calculated and geometric far-field results, shows the resonator to be nearly diffraction limited.

In order to model an unstable resonator containing a grooved mirror and active gain, as accurately as possible, we modified the computer program so that it would be possible to add a phase disturbance to the field intensity after every reflection from the back mirror, and

included only in the $M = 1.2$ resonator) a uniform-saturable gain medium having the following characteristics

$$g = \frac{g_o}{1 + \frac{I}{I_o}} \quad (V-1)$$

where g_o is the small-signal gain, I_o is the saturation flux density, and I is the cavity flux density. For our calculations we assumed $g_o = 2.5\%$ /cm (this is similar to the average small-signal gain shown in Fig. IV-4) and $I_o = 1 \text{ W/cm}^2$.

For the experiment, we used sharp edged grooves in the mirrors. However, because our calculation procedure does not permit infinitely sharp perturbations in field intensity or phase, we used the tapered grooves shown in Fig. V-8.

We tried several groove depths for the 30% coupled resonator before settling on a depth which gave a maximum total phase shift $R_m = 0.8$ rad (actual groove depth of 0.6×10^{-4} cm). A $R_m = 1.4$ rad caused a multimode condition, while 1.1 rad permitted single mode operation but caused severe distortion of the near- and far-field distributions. The perturbed near-field intensity and phase distributions, and far-field intensity distribution are shown in Fig. V-9.

In comparing the perturbed near field with the empty cavity near field in Fig. V-6(a), we can see that the gain medium has expanded the mode volume to more uniformly fill the resonator. While the gain acts to improve the distribution, the grooves cause significant distortion. We can see that close to the center line of each groove the intensity falls nearly to zero, and in the center of the cavity the mode is considerably more structured than for the empty cavity conditions. The effect of the disturbance can easily be seen in the phase distribution, where the profile takes on the appearance of a gaussian near the center of the grooves. In the far-field distribution, the two grooves create large secondary peaks, oriented perpendicular to the grooves, one each side of the central peak. These peaks are similar

3503-45

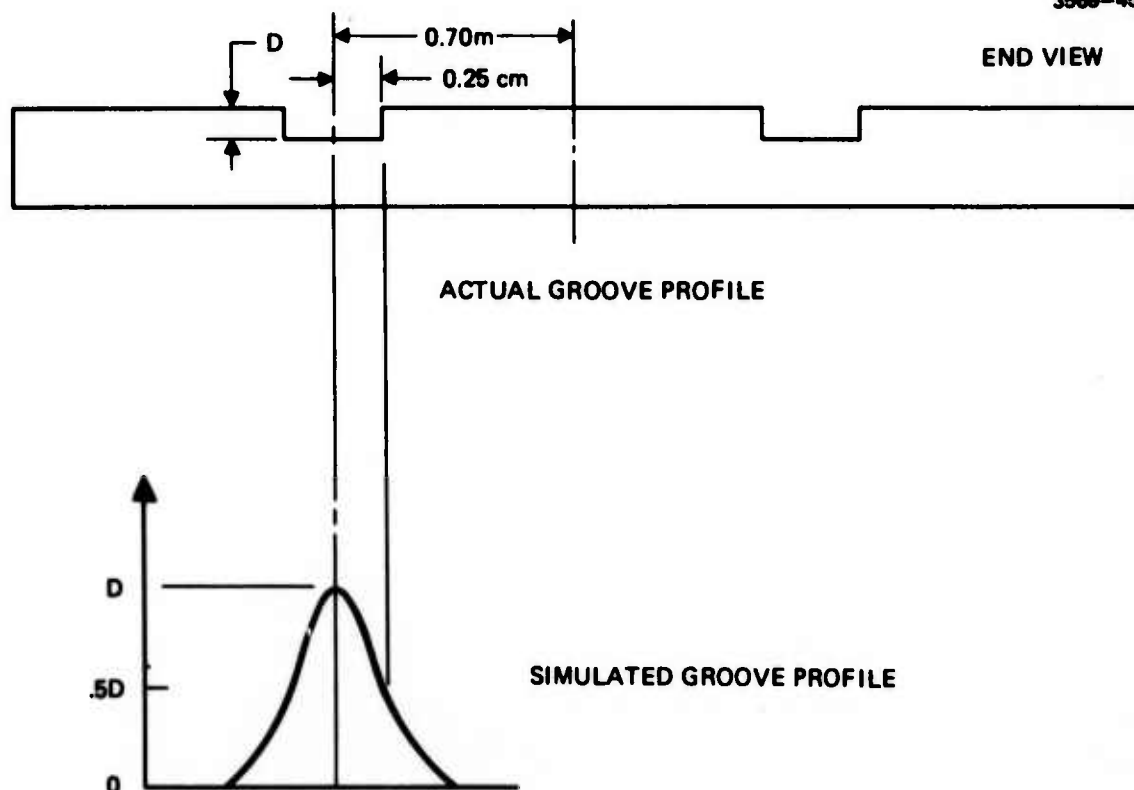
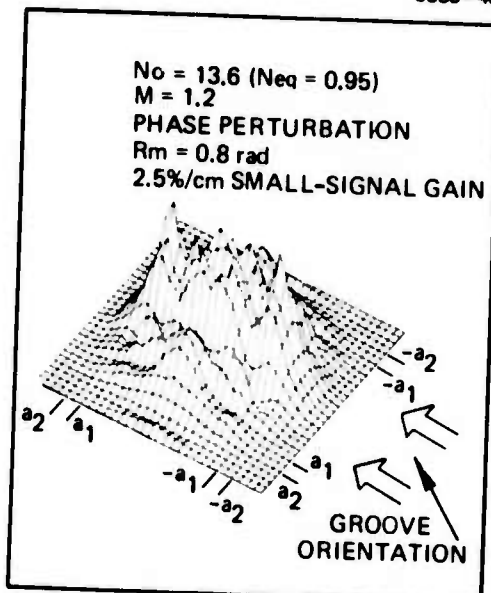


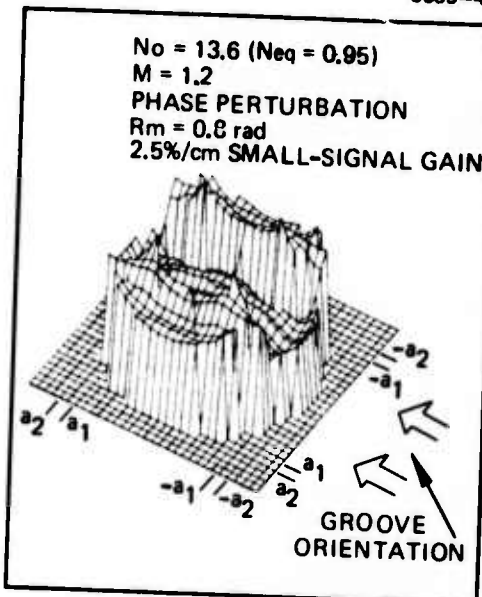
Fig. V-8. Diagram showing profile used in computer program to simulate mirror groove for phase perturbation study.

3569-46

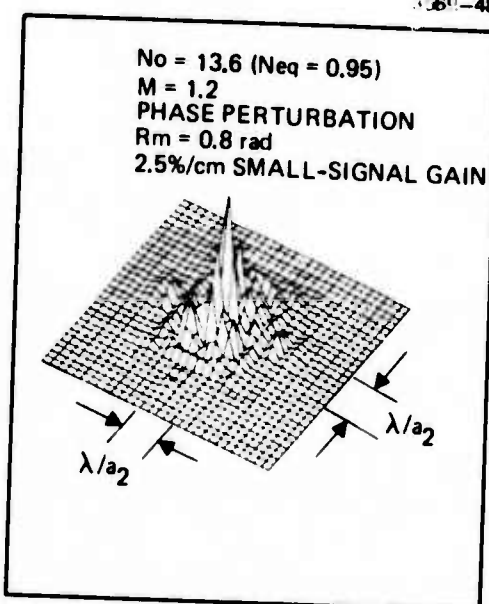


a. NEAR FIELD INTENSITY

3569-47



b. NEAR FIELD PHASE



c. FAR-FIELD INTENSITY

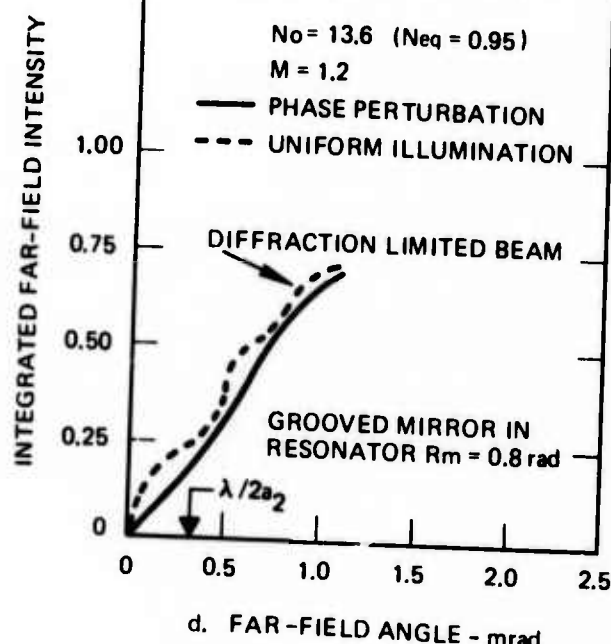


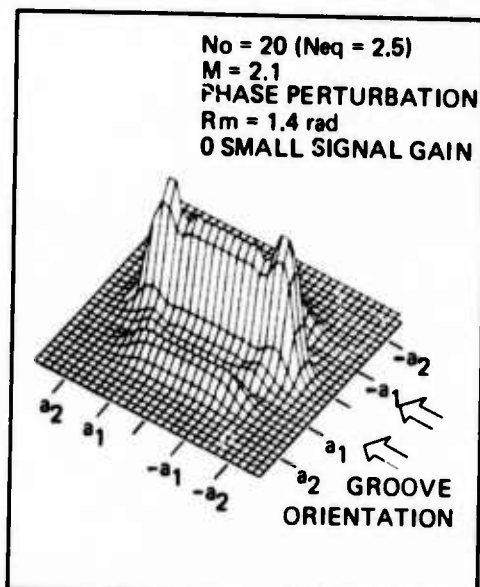
Fig. V-9. Calculated mode distribution for confocal unstable resonator $N_{eq} = 0.95$, $M = 1.2$ (grooved mirrors).

to those found on GDL's where the supersonic shock waves cause a cylindrical lens effect in the cavity, resulting in increased beam divergence in a direction transverse to the medium flow. The effect of the grooves on the integrated far-field intensity can be seen in Fig. V-9(d), where we have compared the empty and perturbed cavity results. For the nonperturbed far-field, approximately 22% of the total power is contained in the central peak. For the perturbed results it drops to 11%. If we include the power in the first side lobe, the perturbed results increase to 85% of the ideal value.

Because unstable resonators become less sensitive to phase perturbations as M increases (larger output coupling), we increased the maximum optical phase shift R_m to 1.4 rad for the 77% coupled resonator calculation. The steady-state near-field intensity and phase distributions, the far-field intensity distribution, and the integrated far-field distribution for the $N_{eq} = 2.5$, $M = 2.1$ (77% coupling loss) are shown in Fig. V-10. The calculations were made assuming the large mirrors contained the groove depth profile shown in Fig. V-8, and the laser medium was nonsaturable with uniform gain. The effect of the grooves on the near-field intensity and phase is similar to what was found for the 30% coupled resonator. There is a null on the intensity profile near the center of the grooves, the phase assumes a gaussian profile at the same location, and the far-field distribution shows increased side lobe power in the direction perpendicular to the grooves. The amount of distortion in the far-field is indicated in the integrated far-field distribution. The amount of perturbed power in the central lobe is only 45% of the power in a diffraction limited beam.

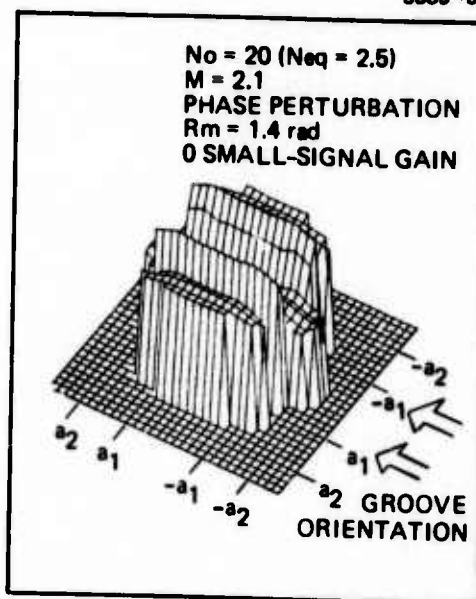
From our calculated results, we choose a groove depth for the experimental measurements which gave an optical phase shift $R_m = 0.8$ and 1.2 rad for the 30% and 77% coupled resonators, respectively. The experimental results for these groove depths are given in the following section.

3569-50



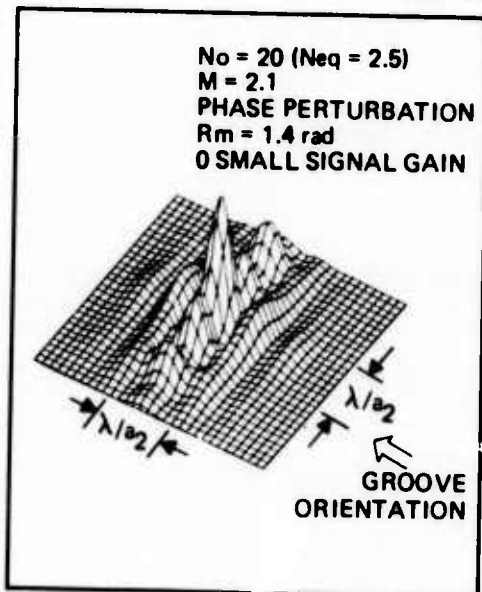
a. NEAR FIELD INTENSITY

3569-51



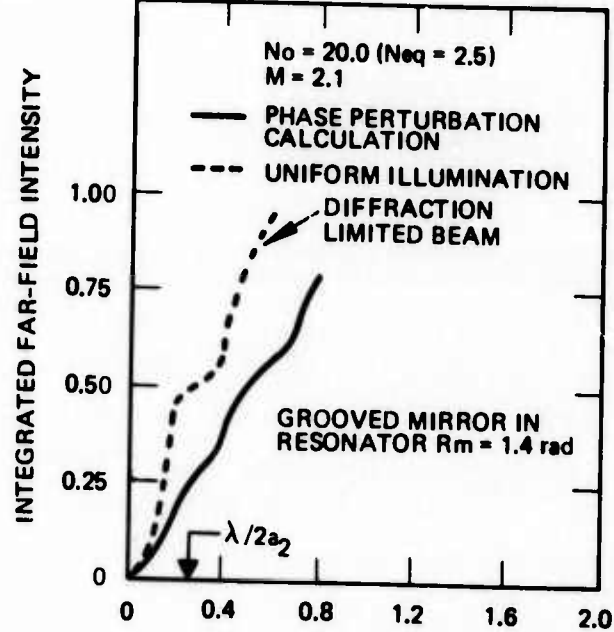
b. NEAR FIELD PHASE

3569-52



c. FAR-FIELD INTENSITY

3569-53



d. FAR-FIELD ANGLE, mrad

Fig. V-10. Calculated mode distributions for confocal unstable resonator $N_{eq} = 2.5$, $M = 2.1$ (grooved mirror).

C. Experimental Results for Perturbed Unstable Resonators

The near-field mode pattern for the 77% ($m = 2.1$) loss coupled resonator and $N_{eq} = 2.1$ is shown in Fig. V-11. The intensity pattern shows the symmetric pattern from the mirror support spider and an intensity null located along the center line of the mirror grooves. The latter disturbance agrees with the intensity nulls found in the calculated near-field distribution in Fig. V-10(a). Figure V-12 shows the far-field mode pattern for the resonator configuration $N_{eq} = 2.5$, $M = 2.1$. The symmetry of the central lobe is relatively undisturbed while the first and second secondary lobes show the same type of asymmetry found in our calculated results in Fig. V-10(c). The mirror grooves cause the power in the side lobes to increase along a line which is perpendicular to the orientation of the grooves.

A quantitative measure of the far-field distortion is shown in Fig. V-13. We can see that due to the grooves, the measured power in the central lobe has decreased approximately 50%. The resonator configuration $N_{eq} = 2.1$ has a slightly higher percentage of its power in the central lobe than $N_{eq} = 2.5$, but this is because the mirror grooves for this resonator are located farther outside the small or feedback mirror, and therefore, less of the phase disturbance is magnified by the resonator. The total power in the central and first side lobe for $N_{eq} = 2.1$ is approximately 71%, down 11% from the value calculated in Fig. V-2 for the non-perturbed resonator. Our calculated results for the integrated far-field power (repeated from Fig. V-10(d)) shows good agreement with the measured power in the central lobe, but too low for the secondary lobes.

Similar results for the 30% ($M = 1.2$) loss coupled resonator, $N_{eq} = 1.2$ and 1.5 are shown in Fig. V-14. The measured central lobe intensity is down approximately 50% from the diffraction limited results, and the sum of the central and first side lobe is down approximately 40%. We can see that the calculated and measured results are in good agreement.

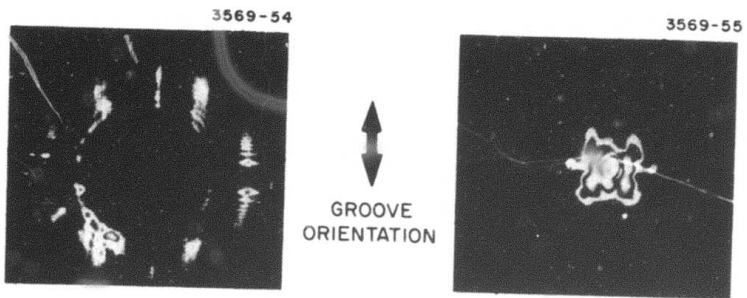


Fig. V-11.
Near-field mode
pattern for un-
stable resonator
with grooved mir-
rors, $N_{eq} = 2.1$,
 $M = 2.1$.

Fig. V-12.
Far-field mode
pattern for
unstable resona-
tor with grooved
mirrors, $N_{eq} = 2.5$,
 $M = 2.1$.

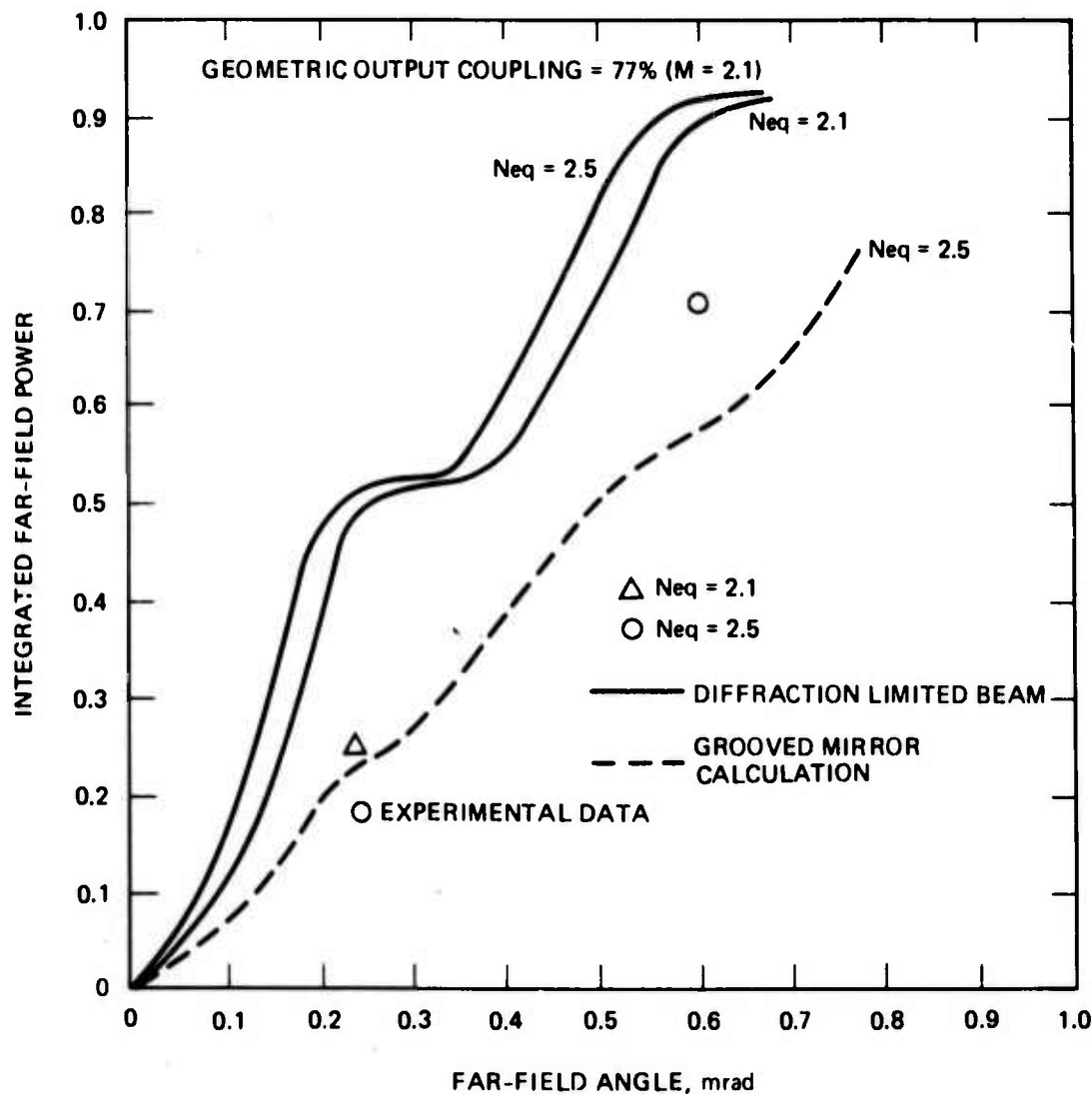


Fig. V-13. Comparison of calculated and measured far-field power for perturbed unstable resonator, $M = 2.1$, $\text{Neq} = 2.5$ and 2.1.

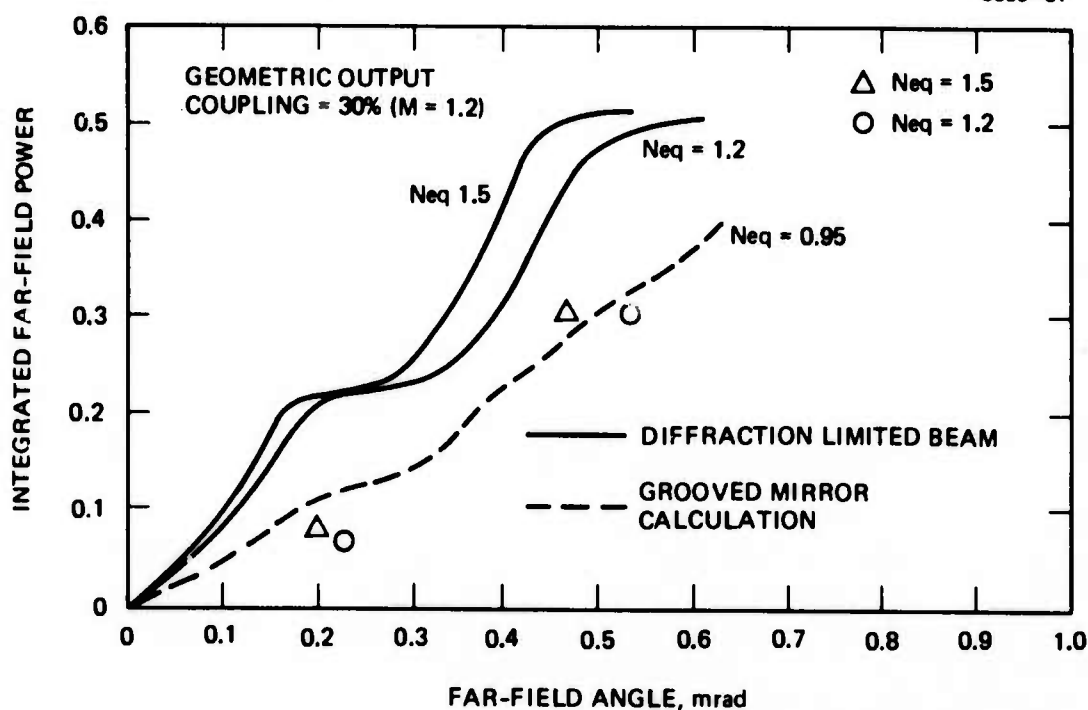


Fig. V-14. Comparison of calculated and measured far-field power for perturbed unstable resonator, $M = 1.2$, $N_{eq} = 1.2$ and 1.5 .

From the results presented in Figs. V-12 and V-13, we can conclude that there is no apparent dependence of beam quality on Fresnel number when significant phase perturbations exist in the laser cavity.

D. Discussion of Experimental and Theoretical Results

Unstable resonator beam quality measurements for resonator geometric magnifications M ranging from 1.2 to 2.1 (loss coupling varies from 30% to 77%) and equivalent Fresnel numbers N_{eq} from 0.95 to 2.5 have been shown in this study to be independent of resonator Fresnel number. The beam quality measurements included laser conditions where roundtrip medium gain ($2 g_o L$, where g_o is the small-signal gain) exceeded oscillating threshold by a factor of 10 for the 30% loss coupled resonators, and conditions where cavity phase disturbances as large as 1.4 rad per roundtrip were introduced into the resonator.

These experimental results seem to support our analytical calculations that good optical beam quality is a result of single transverse mode operation. Our calculations for non-perturbed unstable resonators show no dependence for single mode operation on resonator Fresnel number. We cannot, however, unequivocally state that the beam quality we obtained was a result of single-mode operation. It could be that higher-order modes in unstable resonators have similar properties as the lowest-order mode. To the operator of an unstable resonator who desires good beam quality, the above unresolved question is not of importance.

We should note here that while our experimental results generally agreed with the calculated mode pattern, (all calculations show single transverse mode operation) we did observe what appeared to be oscillations of higher azimuthal ($l \neq 0$) modes. The near-field detector output for some of the laser pulses showed a high frequency oscillation. The depth of modulation was typically less than 15 to 20%, the frequency ≥ 2 MHz, and the appearance of the oscillation occurred at both integer and integer plus one-half values of N_{eq} . The measured beam quality was not noticeably degraded when the oscillations appeared.

Krupke and Sooy¹¹ found that small mirror misalignment ($\approx 10 \mu\text{rad}$) would cause the higher order azimuthal modes to oscillate. Since our resonator mirrors could not be aligned consistently better than $10 \mu\text{rad}$, the oscillations in the near-field detector output were probably a result of higher order azimuthal modes.

REFERENCES

1. A. E. Siegman and R. W. Arrathoon, IEEE J. Quantum Electron. QE-3, 156 (1967).
2. A. E. Siegman and H. Y. Miller, Appl. Opt. 9, 2729 (1970).
3. A. E. Siegman, Proc. IEEE 53, 277 (1965).
4. R. L. Sanderson and W. Streifer, Appl. Opt. 8, 2129 (1969)
5. P. Horwitz, "Asymptotic Theory of Unstable Resonator Modes," Avco Everett Research Laboratory Report AMP 376, May 1973.
6. Chemical Laser Mode Control Program, Final Technical Report, Hughes Research Laboratory, 28 July 1971 through 31 July 1972, Contract DAAH01-72-C-0067
7. Chemical Laser Mode Control Program, Final Technical Report, Hughes Research Laboratory, 13 Nov 1972 through 12 November 1973, Contract DAA H01-73-C-0290.
8. A. N. Chester, Appl. Opt. 12, 2353 (1973)
9. D. B. Rensch and A. N. Chester, Appl. Opt. 12, 997 (1973).
10. H. Granek and A. J. Morency, Appl. Opt. 13, 368 (1974).
11. W. F. Krupke and W. R. Sooy, IEEE J. Quantum Electron. QE-5, 575 (1969)

Preceding page blank